JOURNAL OF PETROLOGY | VOLUME 0 | NUMBER 0 | PAGES 1–32 | 2010 | doi:10.1093/petrology/egq033
Journal of Petrology Advance Access published July 1, 2010

Petrogenesis of the Eocene Tamazert Continental Carbonatites (Central High Atlas, Morocco): Implications for a Common Source for the Tamazert and Canary and Cape Verde Island Carbonatites

MOHAMMED BOUABDELLAH[1]*, KAJ HOERNLE[2], ABDELFETAH KCHIT[1], SVEND DUGGEN[2,3], FOLKMAR HAUFF[2], ANDREAS KLÜGEL[4], DAVID LOWRY[5] AND GEORGES BEAUDOIN[6]

[1]LABORATORY OF MINERAL DEPOSITS, HYDROGEOLOGY AND ENVIRONMENT, DEPARTMENT OF GEOLOGY, FACULTY OF SCIENCES, B.P. 524, 60000 OUJDA, MOROCCO

[2]IFM-GEOMAR, LEIBNIZ-INSTITUTE OF MARINE SCIENCES, RESEARCH DIVISION DYNAMICS OF THE OCEAN FLOOR, WISCHHOFSTR. 1–3, 24148 KIEL, GERMANY

[3]A. P. MØLLER SKOLEN, UPPER SECONDARY SCHOOL OF THE DANISH NATIONAL MINORITY IN GERMANY, FJORDALLEE 1, 24837 SCHLESWIG, GERMANY

[4]UNIVERSITÄT BREMEN, FACHBEREICH 5—GEOWISSENSCHAFTEN, POSTFACH 33 04 40, 28334 BREMEN, GERMANY

[5]DEPARTMENT OF EARTH SCIENCES, ROYAL HOLLOWAY UNIVERSITY OF LONDON, EGHAM TW20 0EX, UK

[6]DEPARTEMENT DE GEOLOGIE ET DE GENIE GEOLOGIQUE, UNIVERSITE LAVAL, QUEBEC (QC), G1K 7P4, CANADA

RECEIVED JANUARY 17, 2009; ACCEPTED JUNE 2, 2010

The Tamazert Eocene alkaline complex of the Central High Atlas Range of Morocco hosts the largest outcropping occurrences of carbonatites in northern Africa. The complex consists of carbonatites and undersaturated ultramafic to syenitic alkaline to peralkaline silicate rocks. Mineralogically and geochemically the Tamazert carbonatites are classified as calciocarbonatites, magnesiocarbonatites and silicocarbonatites. They are enriched in light rare earth elements and large ion lithophile elements (Cs, Rb, Ba, U, Th), but depleted in high field strength elements (particularly, Ti, Nb and Ta). Stable and radiogenic isotope ratios vary in the range of $\delta^{13}C_{PDB} = -5{\cdot}8$ *to 1·8‰,* $\delta^{18}O_{SMOW} = 6{\cdot}9–23{\cdot}5$‰, *initial* $^{87}Sr/^{86}Sr = 0{\cdot}7031–0{\cdot}7076$, $^{143}Nd/^{144}Nd = 0{\cdot}5125–0{\cdot}5129$ *and* $^{206}Pb/^{204}Pb = 18{\cdot}29–19{\cdot}89$. *Calciocarbonatites intruding Jurassic limestones have the highest* $\delta^{13}C$ *and* $\delta^{18}O$ *values and the most radiogenic initial* $^{87}Sr/^{86}Sr$, *but least radiogenic* $^{143}Nd/^{144}Nd$, $^{206}Pb/^{204}Pb$ *and* $^{208}Pb/^{204}Pb$ *isotope ratios, and are interpreted to have interacted with the limestones (crustal components). The magnesio- and silicocarbonatites have Sr, Nd and Pb isotope ratios that are nearly identical to those of low-*$^{87}Sr/^{86}Sr$ *calciocarbonatites. The isotope signature of the high-Sr, low-*$^{87}Sr/^{86}Sr$ *calciocarbonatites with mantle-type O and C isotopic compositions indicates the presence of HIMU- and EMI-type components in the mantle source of the Tamazert carbonatites, similar to what has been proposed for the Cape Verde and Canary Islands. The close similarity in carbonatite composition between the Cape Verde and Canary Islands and Tamazert suggests a common sublithospheric source for these carbonatites. We therefore propose that the Tamazert carbonatites originated through melting of Canary plume material that may have*

*Corresponding author: mbouabdellah2002@yahoo.fr

flowed through a sub-lithospheric corridor extending from the Atlantic near the Canary Islands to the Middle Atlas, formed by the delamination of the subcontinental lithosphere in response to Africa–Europe collision at c. *42 Ma. Seismic tomography data suggest that the common source may be within the lower mantle at depths > 1000 km.*

KEY WORDS: *carbon isotopes; carbonatite; crustal contamination; igneous petrology; isotope; mantle plume; Nd isotopes; oxygen isotopes; Pb isotopes; Sr isotopes*

INTRODUCTION

Cenozoic to Quaternary alkaline-dominated intraplate igneous activity in the Mediterranean area reflects the response of the upper mantle to the complex geodynamic evolution of this vast region, characterized by multiple diachronous continent–continent collision, subduction, delamination and rifting events (Lustrino & Wilson, 2007). Within such a complex geodynamic framework, NW Africa was the site of extensive alkaline magmatism from *c.* 45 Ma to the present, covering much of the Atlas system and its adjacent Precambrian basement terranes. Carbonatite bodies, however, formed exclusively in Morocco (Siroua, Taourirt and Tamazert, described herein) and the Canary and Cape Verde Archipelagos (Bernard-Griffiths *et al.*, 1991*l*; Hoernle & Tilton, 1991*l*; Hoernle *et al.*, 2002; Wagner *et al.*, 2003; and this study). The NW African plate appears to be the primary area on Earth known to host both oceanic and continental carbonatites.

The Eocene Tamazert alkaline complex of Morocco, the focus of our study, hosts the largest outcropping occurrences of carbonatites in northern Africa. Unlike most known intraplate carbonatites commonly associated with extensional tectonics (Bell *et al.*, 1998), the Tamazert carbonatites in the Central High Atlas formed in a compressional regime, reflecting active convergence between the African and Eurasian plates (Bailey, 1992; Frizon de Lamotte *et al.*, 2009). This 'atypical' geodynamic setting raises the question of carbonatite petrogenesis, mantle source components and the effects of the collisional orogeny on magma generation.

Although volumetrically insignificant, carbonatites are unanimously recognized as important rock types both petrologically, by providing insights into the chemical evolution of the subcontinental lithospheric upper mantle (Bell, 2001*l*; Bell & Tilton, 2001*l*) and recycling of oceanic crust and marine sediments (Hoernle *et al.*, 2002), and economically, as they host many of the world's largest REE-rich, Nb–Fe oxide and Cu–Au deposits (Hitzman *et al.*, 1992; Smith & Henderson, 2000). The genesis of carbonatites, however, remains controversial. Available petrogenetic models can be divided into two groups (Woolley, 2003; Mitchell 2005): (1) direct partial melting of a carbonated peridotitic mantle; (2) closed-system derivation at low pressures from a mantle-derived nephelinitic parental melt, through fractional crystallization and/or liquid immiscibility. Reflecting the global debate on carbonatite genesis, models for the genesis of the Tamazert carbonatites, and their relationship to the associated undersaturated silicic rocks, also range from direct derivation through partial melting of a metasomatized enriched mantle (Mourtada, 1997) to derivation of carbonatites from a common parental magma either by crystal fractionation or liquid immiscibility (Bouabdli *et al.*, 1988; Kchit, 1990; Mourtada *et al.*, 1997). Recently, Marks *et al.* (2008) proposed that the various rock types of the Tamazert complex originated from distinct melt batches derived from a heterogeneously carbonated amphibole-lherzolite mantle source.

Previous studies of the Tamzert complex focused mainly on the silicate rocks and to a lesser extent on the carbonatites. Thus far, only a few carbonatite samples have been analyzed for their major and trace element composition and C–O–Sr–Nd isotope ratios (Bouabdli *et al.*, 1988; Bernard-Griffiths *et al.*, 1991*l*; Mourtada *et al.*, 1997). Here we present the first comprehensive geochemical dataset for the Tamazert carbonatites, combining optical and cathodoluminescence microscopy, major and trace element composition of mineral phases and whole-rock samples, and stable (C, O) and radiogenic (Sr, Nd, Pb) isotope ratios into an integrated petrogenetic scheme. We examine crustal and mantle processes involved in the petrogenesis of the studied carbonatites and provide new constraints on geodynamic and mantle processes of the northwestern African plate.

GEOLOGICAL BACKGROUND

The High Atlas Range of southern Morocco represents a Mesozoic intracratonic rift belt, extending for more than 2000 km in an east–west direction from Morocco to Algeria and Tunisia (Fig. 1), that was subsequently uplifted as a result of Africa–Europe continental collision. The Tamazert Eocene complex lies on the northern side of the Central High Atlas (Fig. 1). The complex was discovered by Dubar (1939) and subsequently explored in the 1950s to 1960s. Agard (1956*a*, 1956*b*, 1960, 1973, 1977) gave the original geological description and published the first detailed geological map providing the basis for further investigations. Thereafter, numerous detailed geological investigations focused on the petrography, whole-rock geochemistry and mineral chemistry of the alkaline silicate rocks and to a lesser extent on the associated carbonatites (Aghchmi, 1984; Bouabdli, 1987; Bouabdli *et al.*, 1988; Kadar, 1984; Kchit, 1990; Bernard-Griffiths *et al.*, 1991*l*; Bouabdli & Liotard, 1992; Khadem-Allah, 1993; Khadem Allah *et al.*, 1996, 1998; Mourtada *et al.*, 1997;

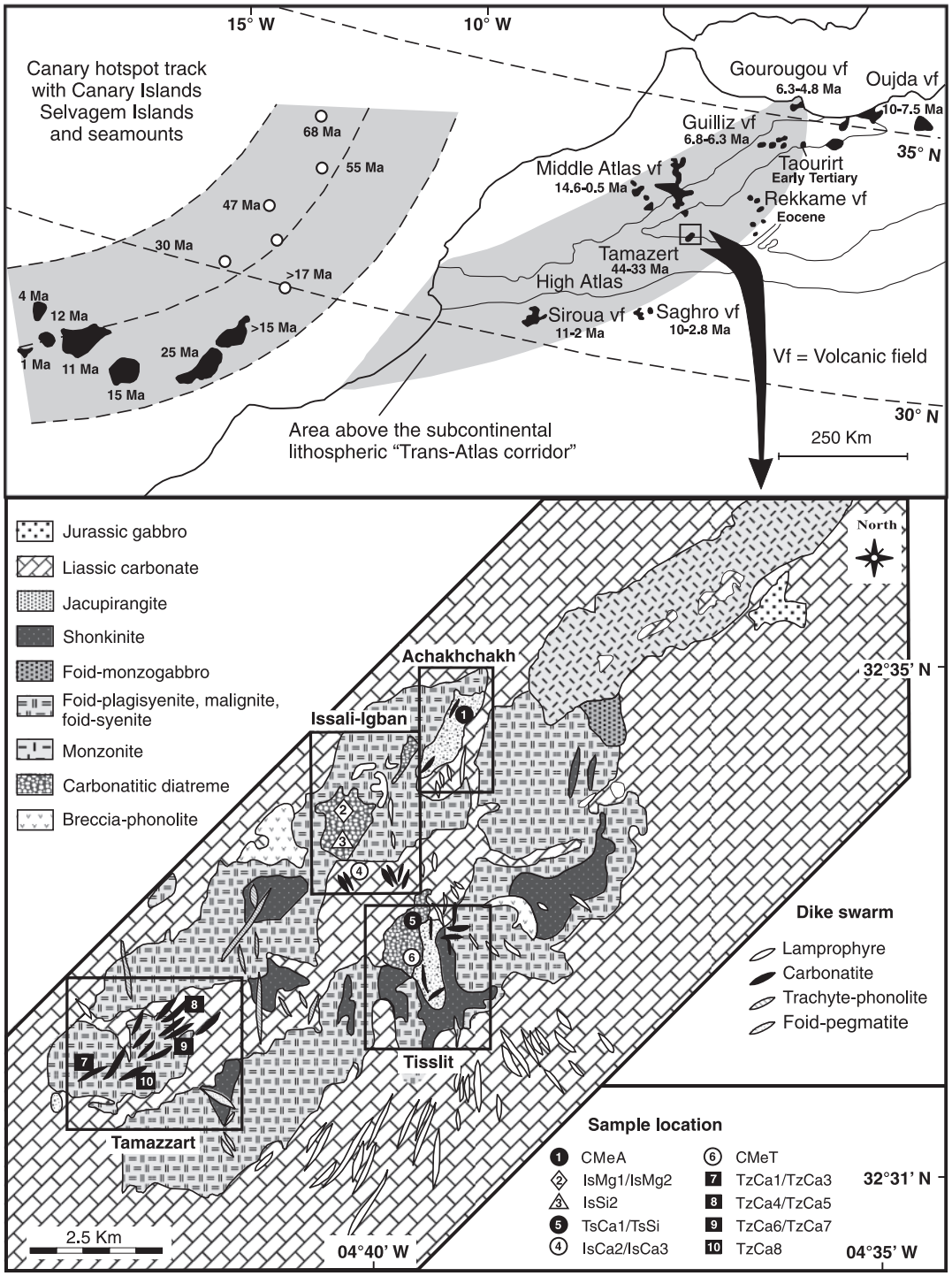

Fig. 1. Geological setting of NW Africa and the Eocene Tamazert igneous complex (modified from Agard, 1973; Kchit, 1990; Duggen *et al.*, 2009). Also indicated are the locations of the studied samples. Radiometric age data sources: Gourougou, Oujda and Guilliz volcanic fields from Hernandez & Bellon (1985) and Duggen *et al.* (2005); Taourirt alkaline lamprophyres and associated carbonatites from Charlot *et al.* (1964) and Wagner *et al.* (2003); Rekkame basanites from Rachdi *et al.* (1997); Middle Atlas from Bellon & Brousse (1977) and Harmand & Cantagrel (1984); Saghro and Siroua from Berrahma & Hernandez (1985) and Berrahma *et al.* (1993).

Al-Haderi *et al.*, 1998; Salvi *et al.*, 2000; Marks *et al.*, 2008; Schilling *et al.*, 2009).

Landsat images, aerial photographs and field observations show that the Tamazert complex is an elongate ENE–WSW-trending 17 km × 5 km elliptical intrusion covering a total area of ~70 km^2 (Fig. 1). The complex consists of silica-undersaturated alkalic rocks and carbonatites that intrude a thick, weakly folded succession of Jurassic platform carbonates, suggesting a shallow depth of intrusion (less than 3 km, Salvi *et al.*, 2000; Marks *et al.*, 2008). Biotite and feldspar separates yielded K–Ar ages of 35 ± 3 Ma and 39 ± 2 Ma for nephelinitic dykes (Klein & Harmand, 1985) and calciocarbonatites (Agard, 1977), respectively; and a Rb/Sr age of 44 ± 4 Ma for monzonites (Tisserant *et al.*, 1976).

Field relationships show that the emplacement of the Tamazert complex is structurally controlled (Mattauer *et al.*, 1977; Kchit, 1990). The complex is intensely faulted, which is responsible for its elongated shape. Khadem Allah *et al.* (1996) compared the morphology of the complex to an 'onion bulb', resulting from the inward cooling of a magma chamber rather than from fracture-driven magmatic injection. The oldest silicate plutonic rocks consist of alkaline ultramafic cumulates and associated differentiated alkaline rocks. The petrography and mineralogy of these rocks has been discussed in detail in the literature (Agard, 1960, 1973, 1977; Bouabdli, 1987; Bouabdli *et al.*, 1988; Kchit, 1990; Bouabdli & Liotard, 1992; Marks *et al.* 2008; Schilling *et al.* 2009) and will not be repeated here. Based on structural relationships, Kchit (1990) and Al-Haderi *et al.* (1998) proposed the following sequence of emplacement: alkaline ultramafites (jacupirangite, biotite-bearing ultramafites, melteigites, ijolites), shonkinites, foid-monzogabbros, foid-plagiosyenites, malignites, nepheline syenites and monzonites. The last stage of magmatic activity, at about 33 Ma, is represented by the intrusion and/or extrusion of a variety of multiply oriented dike arrays containing carbonatites, lamprophyres, porphyritic trachytes, tinguaites and phonolites, and associated hypovolcanic carbonatitic diatremes. Silicate rocks form the major part of the complex, whereas carbonatites constitute less than 10% of the total outcrop area, consistent with what it is commonly observed in carbonatite–alkaline complexes worldwide Barker (1989).

Carbonatites crop out in the southwestern (Tamazzart area) and central parts (Issali-Igban and Tisslit areas) of the complex (Fig. 1), both as intrusive and extrusive occurrences cutting across the nepheline syenitic (*sensu lato*; *s.l.*), the alkaline ultramafic and the Jurassic carbonate wall-rocks.

In this study we follow the carbonatite nomenclature proposed by Gittins & Harmer (1997) and Le Maitre (2002). Intrusive carbonatites are either associated with silicate ultramafic cumulates of the plutonic suite (i.e. melteigites) or the hypovolcanic suite. Melteigite rocks are associated with the alkaline ultramafic pyroxenites of the Achakhchakh area to the north and Tisslit area to the south (Fig. 1), which host numerous occurrences of white, coarse-grained, carbonatitic breccia- to stockwork-like textured plugs (Fig. 2). These rocks were previously described as 'carbonate-bearing silicate rocks' (Agard, 1960) or as 'garnet and calcite-bearing melteigites' (Kchit, 1990).

In contrast, carbonatite occurrences associated with the hypovolcanic suite rocks are widespread throughout the Tamazzart, Issali-Igban and Tisslit areas (Fig. 1). They occur as stocks and swarms of sub-parallel, variable grain-size dikes and branching veins extending laterally within their host silicate rocks over several hundreds of meters along strike. The dikes and veins crosscut sharply either the alkaline ultrabasites, the nepheline syenite (*s.l.*), and/or the Liassic limestones. The wall-rocks are fenitized to a width of 10–20 cm, giving rise to a mineralogical assemblage of sodic amphiboles, phlogopite and albite. In the Issali-Igban and Tisslit areas, the vein system strikes north–south, whereas in the Tamazzart area, the veins strike NE–SW and dip to the NE at an angle of ~80°. Single dikes vary in thickness from a few millimeters to *c.* 4 m. The coarse-grained carbonatite dikes (30–50 cm thick) are intruded by several thin, fine-grained carbonatite veins, suggesting repeated phases of carbonatite intrusion. Similarly, some of the veins exhibit crustiform sheeted structures with symmetrical ribbons of pegmatitic carbonatite, indicating successive vein-opening and vein-filling episodes.

In addition to the intrusive carbonatites, the Tamazert complex in the Issali-Igban and Tisslit areas is characterized by the presence of various occurrences of extrusive carbonatites, in the form of diatreme-like structures. They consist of NE–SW-trending, 700–1400 m long and 300–800 m wide, yellow–brown carbonatitic breccia pipes, cutting across the nepheline syenite (*s.l.*), the ultramafic rocks, the lamprophyres and the Liassic limestones.

SAMPLE PREPARATION AND ANALYTICAL METHODS

Approximately 100 samples were studied by standard thin-section petrography, including staining by alizarin red and potassium ferricyanide. Of these, about 18 samples were studied under the cathodoluminescence microscope and selected for geochemical analysis. An overview of the mineral phases found in the carbonatite samples is outlined in Table 1.

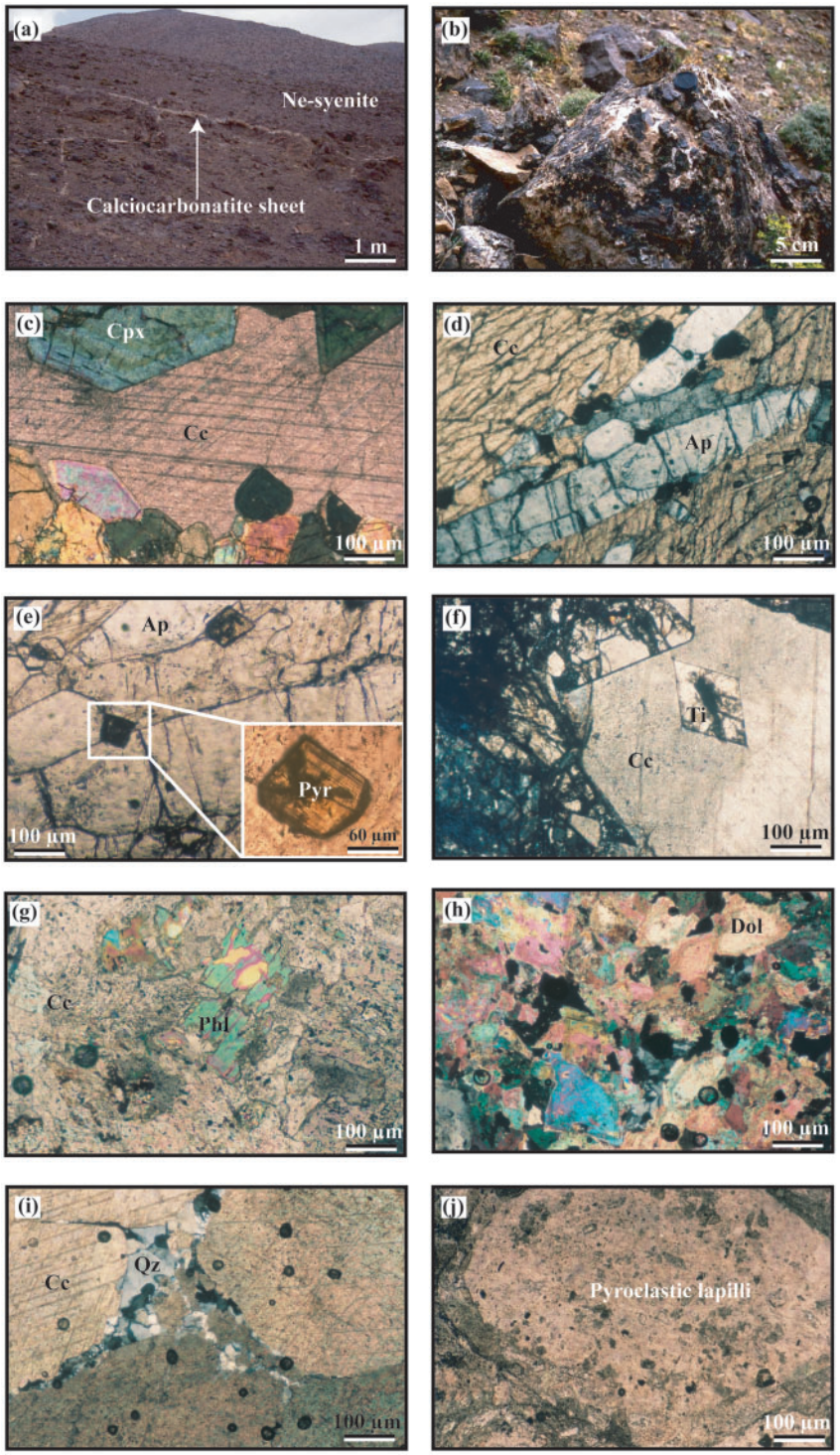

Fig. 2. Field photographs of typical outcrops (a, b) and thin-section photomicrographs (c–j; cross-polarized light) showing the representative carbonatite types, specific textures and mineral associations from the Tamazert complex. (a) Field view of slightly inclined sub-horizontal calciocarbonatite sheet crosscutting the nepheline syenite host-rock in the Tamazzart area. (b) Silicate–carbonate-bearing rock showing chaotic, non-directional vein brecciation of the melteigite-hosted rock (dark material) by veinlet network (stringers) of calciocarbonatite (white material). The field of view is *c.* 1 m × 0·5 m. (c) Coarse-grained melteigite–carbonate-bearing rock showing large subhedral diopside (Cpx) with interstitial (intercumulus) calcite. Calcite is restricted to the interstices between the mafic silicate minerals. (d) Medium-grained calciocarbonatite showing bladed and foliated calcite and associated euhedral prismatic apatite. (e) Medium-grained calciocarbonatite with euhedral zoned pyrochlore (darker brown and higher relief). (f) Medium-grained calciocarbonatite with euhedral titanite. (g) Sub-euhedral phlogopite phenocryst in medium-grained calciocarbonatite exhibiting distinct porphyritic texture. (h) Coarse-grained magnesiocarbonatite showing large zoned rhombs of dolomite with interstitial hydrothermal quartz. (i) Coarse-grained silicocarbonatite containing cumulus calcite crystals lined with hydrothermal quartz and feldspar grains. (j) Iron-rich matrix-supported polymicritic breccia interpreted to be an accretionary lapilli and block tuff from a diatreme structure in the Taourirt area. Ap, apatite; Cc, calcite; Cpx, clinopyroxene; Dol, dolomite; Phl, phlogopite; Pyr, pyrochlore; Qz, quartz; Ne, nepheline; Ti, titanite.

Table 1: Petrographic description and mineral composition of the Tamazert carbonatites

Carbonatite type, locality	Mode of occurrence	Petrography	
		Texture	Main mineral composition
Calciocarbonatites			
TzCa1 (Tamazzart area)	Crustiform vein	Coarse-grained carbonatite (sövite) intruding Ne-syenite	Cc, Ap, Phl, Pyr, REE-carbonates and phosphates
TzCa3 (Tamazzart area)	Dyke, vein	Fine-grained gray calcite fillling interstices managed by white calcite	Cc, Ap, Phl, Pyr, REE-carbonates and phosphates
TzCa4 (Tamazzart area)	Dyke, vein	Pegmatitic-textured calcite (sövite)	Cc, Ap, Phl, Pyr, REE-carbonates and phosphates
TzCa5 (Tamazzart area)	Crustiform vein	Fine-grained gray calcite grading outward into coarse-grained white calcite (sövite)	Cc, Ap, Phl, Pyr, REE-carbonates and phosphates
TzCa7 (Tamazzart area)	Dyke, vein	Medium-grained gray calcite (sövite)	Cc, Ap, Phl, Pyr, REE-carbonates and phosphates
TzCa6 (Tamazzart area)	Crustiform vein	Flat-lying alvikite sheet grading outward into white sövite	Cc, Ap, Phl, Pyr, REE-carbonates and phosphates
TzCa8 (Tamazzart area)	Dyke, vein	Fine-grained calcite (alvikite) intruding Ne-syenite	Cc, Ap, Phl, Pyr, REE-carbonates and phosphates
TsCa1 (Tisslit area)	Dyke, vein	Coarse-grained white carbonatite (sövite) intruding Ne-syenite	CC, Ap, Ti
IsCa1 (Issali-Igban area)	Dyke, vein	Coarse-grained white carbonatite (sövite) intruding Liassic limestone country rock	CC, Phl, Qz
IsCa2 (Issali-Igban area)	Dyke, vein	Fine-grained white carbonatite (sövite) intruding Liassic limestone country rock	CC, Phl, Qz
IsCa3 (Issali-Igban area)	Dyke, vein	Fine-grained white carbonatite (microsövite) intruding Liassic limestone country rock	CC, Phl, Qz
CMeT (Tisslit area)	Breccia-like massive bodies	Rhombohedral calcite phenocryst enclosed within melteigite	Cpx, Gt, Ne, Ap, Bt + interstitial Ca
CMeA (Achakhchakh area)	Breccia-like massive bodies	Rhombohedral phenocrysts of calcite enclosed within melteigite	Cpx, Gt, Ne, Ap, Bt + interstitial Ca
Magnesiocarbonatites			
IsMg1 (Issali-Igban area)	Diatreme, pipe-like brecciated bodies	Fine-grained magnesiocarbonatite	Dol, Ank, Cc relicts, Ba, F, Sul, niobio-tantalates, Fk, Qz
IsMg2 (Issali-Igban area)	Diatreme, pipe-like brecciated bodies	Fine-grained magnesiocarbonatite	Dol, Ank, Cc relicts, Ba, F, Sul, niobio-tantalates, Fk, Qz
Silicocarbonatites			
IsSi1 (Issali-Igban area)	Diatreme, oval-shaped bodies	Accretionary pyroclastic lapilli- and block-tuff	Dol, Ank, Fk, Ab, Qz
IsSi2 (Issali-Igban area)	Dyke, vein	Fine-grained carbonatite collapased within the diatreme zone	Dol, Ank, Fk, Ab, Qz
TsSi (Tisslit area)	Dyke, vein	Fine-grained carbonatite cross-cutting sövite	Dol, Ank, Kk, Ab, Qz

Table 2: Representative electron microprobe analyses and structural formula of minerals from the Tamazert carbonatites

Mineral:	Calcite						Dolomite*	Dolomite core*	Dolomite border*	
Sample no.:	TsCa1	TzCa1	TzCa2	TzCa3	TzCa4		TzCa1	B1	B1	IsSi2
Area:	Tisslit	Tamazzart	Tamazzart	Tamazzart	Tamazzart		Tamazzart	Issali Igban	Issali Igban	Issali Igban
Longitude (W):	4°39′3″	4°42′56″	4°42′33″	4°42′50″	4°41′27″		4°42′56″			4°40′23″
Latitude (N):	32°33′9″	32°32′3″	32°32′4″	32°32′6″	32°32′27″		32°32′3″			32°33′40″
$MgCO_3$	0·07	0·19	0·18	0·21	0·23	$MgCO_3$	27·68	39·59	34·50	28·95
$CaCO_3$	103·18	103·73	102·53	100·01	98·90	$CaCO_3$	51·47	53·22	52·77	51·88
$MnCO_3$	0·15	2·01	1·69	0·83	1·97	$MnCO_3$	3·89	1·57	2·07	1·61
$FeCO_3$	0·10	1·04	0·18	0·50	0·56	$FeCO_3$	18·37	5·63	10·66	17·23
$ZnCO_3$	0·04	0·00	0·00	0·00	0·00	$ZnCO_3$	0·22	n.d.	n.d.	0·09
$SrCO_3$	0·5	0·85	0·32	0·62	0·53	$SrCO_3$	0·87	n.d.	n.d.	0·63
$BaCO_3$	0·01	0·04	0·02	0·05	0·00	$BaCO_3$	0·00	n.d.	n.d.	0·00
Sum	104·04	107·86	104·92	102·21	102·18	Sum	102·50	100·01	100·00	100·39
Calculated on the basis of 6 O						*Calculated on the basis of 6 O*				
Mg	0·002	0·004	0·004	0·005	0·005	Mg	0·629			0·667
Ca	1·985	1·934	1·960	1·964	1·944	Ca	0·985			1·007
Mn	0·002	0·033	0·028	0·014	0·034	Mn	0·065			0·027
Fe^{2+}	0·002	0·017	0·003	0·008	0·009	Fe^{2+}	0·304			0·289
Zn	0·001	0·000	0·000	0·000	0·000	Zn	0·003			0·002
Sr	0·007	0·011	0·004	0·008	0·007	Sr	0·011			0·009
Ba	0·000	0·000	0·000	0·000	0·000	Ba	0·000			0·000

Mineral:	Ankerite		Apatite				Phlogopite	
Sample no.:	IsMg ext		TsCa1	TzCa2	TzCa4		CMeA	TsCa2
Area:	Issali Igban		Tisslit	Tamazzart	Tamazzart		Achakhchakh	Tisslit
Longitude (W):	4°40′23″		4°39′3″	4°42′33″	4°41′27″		4°39′15″	4°39′25″
Latitude (N):	32°33′50″		32°33′9″	32°32′4″	32°32′27″		32°34′50″	32°33′3″
$MgCO_3$	24·35	MgO	0·07	0·04	0·05	MgO	19·08	15·10
$CaCO_3$	49·20	CaO	54·48	52·65	53·28	CaO	0·10	0·09
$MnCO_3$	3·30	MnO	0·02	0·05	0·03	MnO	1·20	0·73
$FeCO_3$	22·40	FeO	0·02	0·01	0·04	FeO	10·62	16·44
$ZnCO_3$	0·05	SiO_2	0·26	0·10	0·12	SiO_2	40·33	38·27
$SrCO_3$	0·29	Na_2O	0·31	0·40	0·26	K_2O	9·64	9·24
$BaCO_3$	0·01	P_2O_5	37·98	38·51	38·80	TiO_2	0·87	2·70
Sum	99·60	La_2O_3	0·05	0·37	0·21	Al_2O_3	10·58	11·16
		Ce_2O_3	0·10	0·71	0·31	BaO	0·13	0·15
		H_2O	0·00	0·00	0·00	H_2O	3·53	3·34
		F	4·75	6·32	5·02	F	0·91	1·18
		Sum	98·05	99·16	98·12	Sum	97·00	98·40
Calculated on the basis of 6 O		*Calculated on the basis of 24 (O, OH, F)*				*Calculated on the basis of 25 O*		
Mg	0·572	Mg	0·020	0·010	0·013	Mg	4·305	3·456
Ca	0·980	Ca	10·301	9·832	10·026	Ca	0·016	0·015
Mn	0·057	Mn	0·003	0·008	0·004	Mn	0·154	0·095
Fe^{2+}	0·386	Fe^{2+}	0·004	0·002	0·006	Fe^{2+}	1·346	2·112
Zn	0·001	Si	0·046	0·018	0·021	Si	6·106	5·877
Sr	0·004	Na	0·107	0·137	0·089	K	1·863	1·811
Ba	0·000	P	5·675	5·682	5·768	Ti	0·099	0·312
		La	0·003	0·024	0·014	Al	1·888	2·019
		Ce	0·006	0·046	0·020	Ba	0·008	0·009
		H	0·000	0·000	0·000	F/(F+M)	25·835	38·973
		F	−2·000	−2·660	−2·113			

(continued)

Table 2: Continued

Mineral:	Pyrochlore			K-Feldspar				Titanite
Sample no.:	TzCa2	TzCa4		TzCa3	TzCa6	IsMg ext		TsCa2
Area:	Tamazzart	Tamazzart		Tamazzart	Tamazzart	Issali Igban		Tisslit
Longitude (W):	4°42′33″	4°41′27″		4°42′50″	4°41′28″	4°40′23″		4°39′25″
Latitude (N):	32°32′4″	32°32′27″		32°32′6″	32°32′	32°33′50″		32°33′3″
FeO	0·19	0·04	SiO_2	64·19	64·42	64·07	SiO_2	30·56
La_2O_3	0·72	0·40	Al_2O_3	18·79	19·05	19·20	TiO_2	34·44
Ce_2O_3	2·36	1·26	MgO	0·01	0·03	0·01	Al_2O_3	0·54
Nd_2O_3	0·60	0·25	CaO	0·02	0·12	0·03	MgO	0·00
Ta_2O_5	0·00	0·09	FeO	0·00	0·04	0·04	CaO	27·69
TiO_2	7·13	6·17	Na_2O	0·24	0·63	0·25	MnO	0·02
CaO	13·75	15·13	K_2O	14·20	14·32	13·18	FeO	1·85
Nb_2O_5	59·79	62·48	Sum	97·45	98·62	96·77	H_2O	4·83
ZrO_2	0·67	1·10					Sum	99·96
Na_2O	5·76	7·12						
F	3·84	4·68						
Sum	94·82	98·73						
			Calculated on the basis of 8 O				*Calculated on the basis of 20 (O, OH)*	
			Si	3·004	2·988	3·001	Si	3·790
			Al	1·037	1·041	1·060	Ti	3·212
			Mg	0·001	0·002	0·001	Al	0·078
			Ca	0·001	0·006	0·002	Mg	0·000
			Fe^{2+}	0·000	0·002	0·002	Ca	3·683
			Na	0·021	0·056	0·230	Mn	0·002
			K	0·848	0·847	0·788	Fe^{2+}	0·192
			An	0·00	0·01	0·00	F/(F+M)	99·818
			Ab	0·02	0·06	0·03		
			Or	0·98	0·93	0·97		

*Data from Mourtada (1997).
n.d., not detected.

Mineral and whole-rock major and trace element data

Mineral chemistry data presented in Table 2 were obtained using a five-spectrometer CAMECA SX-100 electron microprobe at Université Laval, Quebec (Canada). Selected minerals were analyzed with an accelerating voltage of 15 kV and a beam current of 20 nA. The beam diameter varied between 1 and 10 μm depending on the volatile abundance in the mineral of interest. Counting time was 20 s on the peak and 10 s on background. International standards of natural materials were used for calibration and all data were reduced with the PAP procedure.

Major and trace element abundances (Ba, Co, Cr, Cu, Ga, Rb, Sr, V and Zr) in whole-rock powders were determined on fused pellets with a Philips X'unique PW 1480 X-ray fluorescence spectrometer (XRF) at IFM-GEOMAR in Kiel (Germany). International reference standards JB-2, JB-3 (basalt), JA-2, JA-3 (andesite), JR-2, JR-3 (rhyolite), JG-2, GM (granite) and JF-1 (feldspar) were analyzed along with the samples. H_2O and CO_2 were measured photometrically with a Rosemont Infrared Photometer CWA 5003. Carbonate standard KH was used for calibration of the photometer and determined together with the samples. Values measured for the KH standard deviated less than 0·34% from the standard value (37·6% CO_2).

Concentrations of TiO_2, Al_2O_3, Na_2O, K_2O and most other trace elements were determined by inductively coupled plasma-mass spectrometry (ICP-MS) on a ThermoFinnigan Element2 at the Institute of Geosciences, University of Bremen (Germany). Pressure digests were prepared by dissolving 50 mg of sample powder in an HF–aqua regia mixture in Teflon beakers at 210°C using a MLS Ethos microwave. Analyte solutions

had a final dilution factor of 1:5000 corresponding to 0·2 mg/ml of total dissolved solid, and were spiked with 1 ng/ml indium as internal standard. To avoid mass interferences, K, Ti and the middle REE (MREE) to heavy REE (HREE) were measured at high resolution (10 000), Na, Al and transition metals at medium (4000) resolution, and all other elements at low (300) resolution. Data were acquired in nine passes with dwell times between 0·12 and 2·4 s for each element. The instrument was calibrated using USGS standard reference material BCR-2 for TiO_2, Al_2O_3, Na_2O and K_2O, and a mixture of pure element standards in various dilutions for all other elements. External precision as determined by repeated processing and analyses of BCR-2 was 5–8% for Li, Ho, Er, Yb and Ta, and 1–5% for other elements. The accuracy of BCR-2 processed and analyzed along with the samples is better than 10%, except for Zn, Y, Hf, Th and U (up to 15%) and Cr and Cu (up to 20%), with respect to the USGS reference values. The whole-rock major and trace element data are reported in Table 3.

Whole-rock stable and radiogenic isotope analyses

Carbon and oxygen isotope analyses were carried out at Royal Holloway University of London (RHUL) using a PRISM dual-inlet mass spectrometer. Approximately 500 μm of powdered carbonate were weighed into stainless steel buckets and inserted into a 44-position carousel. This normally contains 34 unknowns and 10 standards, including NBS-19 international limestone standard and RHBNC internal calcite standard. These drop sequentially into a common bath of orthophosphoric acid and react at 90°C. All samples reacted to completion within the 10 min reaction time. Any water present is removed using a methylated spirit trap and the purified CO_2 frozen into a cold finger at liquid nitrogen temperature. The gas then passes into the mass spectrometer for analysis. The raw mass 44, 45 and 46 data are converted to $\delta^{13}C$ and $\delta^{18}O$ using standard corrections (Craig, 1957). The corrected data have precisions of better than ±0·1‰ for both $\delta^{13}C$ and $\delta^{18}O$. The data are calibrated using the two standards that have values with respect to V-PDB as follows: NBS-19, $\delta^{13}C = +1{\cdot}95‰$ and $\delta^{18}O = -2{\cdot}20‰$ and RHBNC = $\delta^{13}C + 3{\cdot}25‰$ and $\delta^{18}O$ −10·40‰ (calibrated using international standard LSVEC). Isotopic data are reported relative to Vienna SMOW for oxygen and PeeDee Belemnite (V-PDB) for carbon.

Sr–Nd–Pb isotope analyses were carried out by thermal ionization mass spectrometry (TIMS) at IFM-GEOMAR (Germany). Prior to dissolution matrix chips were briefly washed with cold 2M HCl. Digestion of carbonate and silicate phases was achieved with 6M HCl followed by evaporation of the HCl and treatment with a mixture of concentrated HF and HNO_3. Sr was separated and purified by two passes on the Sr Spec extraction resin. The REE were separated from the matrix elements on AG50W-X8 cation exchange resin and Nd was separated from the remaining REE using Eichrom Ln-Spec resin. Pb was separated and purified by two passes on the AG1-X8 anion resin. Sr–Nd isotopic ratios were determined by TIMS on a TRITON system and Pb isotopes on a MAT262 RPQ2+ system. Both instruments operate in static multi-collection mode. Sr and Nd isotopic ratios are normalized within run to $^{86}Sr/^{88}Sr = 0{\cdot}1194$ and $^{146}Nd/^{144}Nd = 0{\cdot}7219$ and all errors are reported as 2σ errors. The Sr isotope data are reported relative to $^{87}Sr/^{86}Sr = 0{\cdot}710250 \pm 0{\cdot}000007$ ($n = 17$) for NBS987, whereas the Nd isotope data are reported relative to $^{143}Nd/^{144}Nd = 0{\cdot}511852 \pm 0{\cdot}00006$ ($n = 6$) for La Jolla. The long-term reproducibility of NBS 981 ($n = 122$) is $^{206}Pb/^{204}Pb = 16{\cdot}898 \pm 0{\cdot}007$, $^{207}Pb/^{204}Pb = 15{\cdot}436 \pm 0{\cdot}009$, $^{208}Pb/^{204}Pb = 36{\cdot}523 \pm 0{\cdot}027$ and data are corrected to the NBS 981 values given by Todt *et al.* (1996), corresponding to mass bias drift correction of 0·109, 0·114 and 0·121%/a.m.u. for $^{206,207,208}Pb/^{204}Pb$, respectively. Total chemistry blanks were <100 pg for Sr, Nd and Pb and thus considered negligible. Stable and radiogenic isotope data are reported in Table 4.

PETROGRAPHY AND MINERALOGY

Petrography

Based on geological occurrence and spatial distribution, rock fabrics and mineral paragenesis, the Tamazert carbonatites are grouped into two main types: calcite carbonatites and dolomite carbonatites (hereafter referred to as calcio- and magnesiocarbonatites, respectively); a third subordinate carbonatite type defined as silicocarbonatite (% carbonates < 50% vol.) is also recognized. More extreme compositions (e.g. ferrocarbonatites and strontianite-bearing carbonatites) have been identified by Mourtada (1997). However, such compositions should be viewed with some caution, particularly in the case of the Tamazert complex, where the primary carbonatite compositions have undergone extensive and pervasive late-stage sub-solidus mineralogical and chemical changes.

Calciocarbonatites are volumetrically dominant (*c.* 50 vol. %) and the most widespread, occurring in the Issali-Igban, Tisslit and Tamazzart areas (Fig. 1). Most of the dikes are <1 to 2 m wide, striking NNE–SSW, east–west and NNW–SSE and >100 m in length along strike. The carbonatitic dikes exhibit evidence of tectonic effects as indicated by the alignment of rock-forming minerals, kinked twin boundaries, curved cleavage and wavy extinction of carbonate phenocrysts.

In thin section, the calciocarbonatites show magmatic to blastic and porphyroblastic textures (Fig. 2). They are commonly fine- (alvikites), medium- (microsövites),

Table 3: Major and trace element composition of Tamazert carbonatites, determined by XRF and ICP-MS

Carbonatite type:	Calciocarbonatites						
Sample no.:	Tz Ca1	Tz Ca5	Tz Ca4	Tz Ca7	Tz Ca3	Tz Ca8	Tz Ca6
Locality:	Tamazzart	Tamazzart	Tamazzart	Tamazzart	Tamazzart	Tamazzart	Tamazzart
Longitude (W):	4°42′56″	4°41′47″	4°41′27″	4°41′33″	4°42′50″	4° 42′16″	4°41′28″
Latitude (N):	32°32′3″	32°32′29″	32°32′27″	32°32′15″	32°32′6″	32°31′57″	32°32′
Major elements (wt %)							
SiO_2	1·25	1·26	1·24	1·33	6·83	1·29	3·62
TiO_2	0·01	0·01	0·01	0·01	0·01	0·01	0·11
Al_2O_3	0·02	0·02	0·01	0·04	0·84	0·02	0·38
FeO_T	0·37	0·55	0·35	0·53	0·46	0·81	3·22
MnO	1·08	1·05	0·54	0·98	0·78	3·06	2·28
MgO	0·42	0·71	0·38	0·56	0·36	0·59	0·56
CaO	54·54	53·70	53·36	52·31	50·28	56·37	47·39
Na_2O	0·01	0·01	0·01	0·02	0·01	0·01	0·03
K_2O	0·00	0·00	0·00	0·02	1·14	0·01	0·48
P_2O_5	0·02	0·06	0·15	0·11	0·02	0·03	1·19
H_2O	0·11	0·07	0·08	0·10	0·07	0·09	0·25
CO_2	42·40	42·85	43·25	43·22	39·06	43·18	38·05
Total	100·20	100·3	99·4	99·2	99·9	105·5	97·60
Trace elements (ppm)							
Li	0·32	b.d.	b.d.	0·33	b.d.	0·67	2·78
V	1·72	11·71	4·18	10·9	4·43	6·96	69·8
Cr	0·18	0·28	0·11	0·27	0·25	0·28	2·80
Co	0·01	0·06	0·02	0·04	0·17	0·04	0·94
Ni	0·02	0·14	0·30	0·04	0·10	0·12	0·48
Zn	10·3	34·2	15·6	23420	18·9	20·0	449
Ga	0·06	0·02	b.d.	0·13	0·69	0·05	1·64
Rb	0·09	b.d.	b.d.	0·43	21·5	0·20	9·08
Sr	15968	21378	20362	27601	12017	26792	36260
Y	136	128	72·00	97·2	185	223	173
Zr	0·92	0·83	1·34	1·94	0·87	0·84	13·44
Nb	0·96	2·43	44·4	85·3	0·41	1·94	915
Cs	0·01	b.d.	b.d.	0·01	b.d.	b.d.	b.d.
Ba	2225	2814	1396	1864	3337	3217	1939
La	983	669	584	459	889	412	3178
Ce	1511	1045	807	679	1342	703	3787
Pr	137	94·0	67·5	61·0	125	66·9	295
Nd	435	300	196	198	409	217	783
Sm	54·6	43·0	24·3	28·7	77·2	31·6	80·9
Eu	15·5	12·7	7·07	8·29	25·4	10·0	22·7
Gd	40.0	33·2	17·5	21·8	63·7	28·4	56·0
Tb	5·21	4·47	2·38	3·04	8·61	5·12	6·79
Dy	29·9	25·5	13·3	18·2	44·3	37·1	37·0
Ho	5·38	4·84	2·57	3·52	7·21	8·21	6·90
Er	14·6	14·1	7·21	10·4	17·2	26·1	20·4
Tm	1·19	2·12	1·05	1·54	2·36	3·97	2·92
Yb	11·4	13·4	6·61	9·88	14·4	26·0	18·7
Lu	1·55	1·87	0·90	1·36	1·91	3·63	2·54
Hf	0·28	0·25	0·16	0·23	0·40	0·31	0·94
Ta	0·05	0·05	0·06	0·21	0·07	0·08	2·46
Pb	20·2	27·1	17·9	22·2	11·9	28·1	64·0
Th	5·81	11·3	2·46	9·35	61·3	20·5	25·5
U	2·87	2·47	2·57	4·56	3·16	0·56	81·3

(continued)

Table 3: Continued

Carbonatite type:	Calciocarbonatites					
Sample no.:	Is Ca1	Is Ca2	Is Ca3	Ts Ca1	CMeT	CMeA
Locality:	Issali Igban	Issali Igban	Issali Igban	Tisslit	Tisslit	Achakhchakh
Longitude (W):	4°40′20″	4°40′8″	4°40′12″	4°39′3″	4°39′35″	4°39′15″
Latitude (N):	32°33′33″	32°33′33″	32°33′38″	32°33′9″	32°32′40″	32°34′40″
Major elements (wt %)						
SiO_2	1·96	1·36	1·44	2·21	1·34	1·3
TiO_2	0·01	0·01	0·01	0·00	0·00	0·01
Al_2O_3	0·02	0·03	0·04	0·02	0·02	0·02
FeO_T	0·16	0·07	0·13	0·18	0·13	0·23
MnO	0·18	0·14	0·14	0·15	0·21	0·10
MgO	0·31	0·63	0·79	0·30	0·32	0·30
CaO	53·6	55·9	55·8	53·2	56·6	51·4
Na_2O	0·02	0·01	0·02	0·01	0·01	0·02
K_2O	0·00	0·02	0·03	0·00	0·00	0·01
P_2O_5	0·02	0·05	0·05	0·03	0·002	0·02
H_2O	0·13	0·16	0·13	0·15	0·04	0·11
CO_2	43·4	44·0	44·3	42·8	44·3	43·5
Total	99·8	102·4	102·9	99·1	103·0	97·0
Trace elements (ppm)						
Li	b.d.	0·37	97·8	b.d.	0·27	0·07
V	1·97	6·37	11·7	3·60	0·38	6·25
Cr	0·05	2·38	2·10	0·22	0·24	0·40
Co	0·02	0·08	0·10	0·02	0·51	0·06
Ni	0·59	0·92	0·70	0·12	0·70	0·04
Zn	16·3	159·8	79·1	11·4	7·27	10·3
Ga	0·02	0·24	0·20	0·02	0·09	0·09
Rb	0·00	0·69	0·68	0·00	0·07	0·21
Sr	14392	1132	1153	12874	2855	27091
Y	11·9	2·81	6·00	9·75	0·75	7·10
Zr	1·12	3·11	4·40	2·03	0·57	3·71
Nb	0·45	0·93	0·96	0·43	0·14	0·36
Cs	b.d.	0·03	0·01	b.d.	0·01	0·01
Ba	1180	9·10	83·6	1182	18·5	1032
La	143	8·74	2·65	113	232	150
Ce	127	8·22	2·43	102	187	180
Pr	8·79	0·53	0·20	7·25	10·6	14·2
Nd	22·5	1·38	0·74	19·0	23·4	40·9
Sm	2·19	0·18	0·16	2·07	0·98	3·60
Eu	0·65	0·06	0·06	0·55	0·23	0·88
Gd	1·52	0·21	0·27	1·36	0·32	2·55
Tb	0·20	0·03	0·07	0·17	0·03	0·23
Dy	1·39	0·25	0·64	1·16	0·13	1·10
Ho	0·32	0·07	0·18	0·27	0·02	0·20
Er	1·11	0·24	0·69	0·86	0·05	0·56
Tm	0·17	0·04	0·13	0·13	0·01	0·08
Yb	1·13	0·26	0·94	0·86	0·04	0·53
Lu	0·18	0·04	0·16	0·13	0·01	0·08
Hf	0·03	0·07	0·09	0·04	0·03	0·09
Ta	0·02	0·03	0·04	0·02	0·02	0·03
Pb	5·81	10·39	10·71	4·75	2·56	8·04
Th	1·70	1·12	1·22	1·36	0·01	0·94
U	0·30	0·75	0·82	0·31	0·03	0·27

(continued)

Table 3: Continued

Carbonatite type:	Magnesiocarbonatites		Silicocarbonatites		
Sample no.:	Is Mg2	Is Mg1	Is Si1	Is Si2	Ts Si
Locality:	Issali Igban	Issali Igban	Issali Igban	Issali Igban	Tisslit
Longitude (W):	4°40′20″	4°40′20″	4°40′12″	4°40′23″	4°39′3″
Latitude (N):	32°33′50″	32°34′6″	32°34′12″	32°33′40″	32°33′
Major elements (wt %)					
SiO_2	1·46	5·61	19·24	25·4	30·79
TiO_2	0·04	0·05	1·73	1·92	1·41
Al_2O_3	0·06	0·04	2·95	1·93	5·47
FeO_T	5·18	3·08	6·92	6·89	6·26
MnO	0·84	1·78	0·72	0·64	0·36
MgO	18·6	18·3	7·78	8·99	6·52
CaO	32·9	30·4	24·4	18·4	15·4
Na_2O	0·03	0·11	0·12	0·05	0·13
K_2O	0·01	0·01	3·95	0·50	5·40
P_2O_5	0·24	0·04	1·43	2·99	0·69
H_2O	0·24	0·37	0·29	1·35	0·7
CO_2	45·4	42·2	26·4	26·0	19·9
Total	105·0	102·0	96·0	95·0	93·0
Trace elements (ppm)					
Li	1·16	10·4	9·74	12·7	4·02
V	484	1485	1134	290	247
Cr	9·16	46·14	184	392	173
Co	3·75	1·94	22·5	28·1	21·6
Ni	30·4	11·7	78·3	142	93·6
Zn	360	10·3	254	278	3010
Ga	0·28	0·19	9·41	8·03	19·7
Rb	0·15	0·36	45·5	9·59	116·4
Sr	1088	5363	1962	17017	2184
Y	98·3	23·4	56·5	68·7	39·2
Zr	3·73	54·2	32·5	238	356
Nb	9·55	4·03	293	372	237
Cs	0·00	0·01	0·05	0·13	0·41
Ba	3987	460	3313	2746	1685
La	527	3412	600	716	324
Ce	637	2917	718	1099	487
Pr	53·6	179	58·6	106	46·6
Nd	161	399	171	342	151
Sm	22·5	31·5	20·0	41·4	20·6
Eu	7·86	7·78	5·87	11·1	5·92
Gd	22·8	16·2	14·4	25·7	14·4
Tb	3·42	1·47	1·88	2·99	1·73
Dy	19·5	5·87	10·7	15·7	9·26
Ho	3·39	0·89	1·87	2·59	1·45
Er	10·6	3·35	5·94	6·71	4·06
Tm	1·76	0·57	0·95	0·81	0·46
Yb	13·5	4·78	7·70	4·56	2·82
Lu	2·20	0·86	1·30	0·60	0·37
Hf	0·19	0·65	1·18	6·46	6·35
Ta	0·07	0·01	3·69	5·12	n.d.
Pb	37·9	44·3	43·1	52·1	n.d.
Th	136	64·3	29·9	62·1	n.d.
U	3·56	10·8	24·6	4·48	n.d.

*n.d., not determined.

Table 4: Stable and radiogenic isotope data of Tamazert carbonatites

Sample	Location	$\delta^{13}C_{PDB}$(‰)	$\delta^{18}O_{SMOW}$(‰)	$(^{87}Sr/^{86}Sr)_{in}$	$^{87}Sr/^{86}Sr$	2SD	$(^{143}Nd/^{144}Nd)_{in}$	$^{143}Nd/^{144}Nd$	2SD	$(^{206}Pb/^{204}Pb)_{in}$	$^{206}Pb/^{204}Pb$	2SD	$(^{207}Pb/^{204}Pb)_{in}$	$^{207}Pb/^{204}Pb$	2SD	$(^{208}Pb/^{204}Pb)_{in}$	$^{208}Pb/^{204}Pb$	2SD
Calciocarbonatites																		
CMeT	Tisslit	−4·92	8·52	0·705695	0·705695	3	0·512647	0·512655	3	18·804	18·828	0·001	15·575	15·611	0·001	38·739	38·884	0·003
Is Ca2	Issali-Igban	1·74	23·50	0·707543	0·707544	3	0·512541	0·512565	41	18·276	18·329	0·002	15·568	15·605	0·002	38·221	38·381	0·004
Is Ca3	Issali-Igban	0·90	19·46	0·707585	0·707586	3	0·512587	0·512627	14	18·436	18·492	0·003	15·565	15·602	0·002	38·343	38·504	0·006
Tz Ca8	Tamazzart	−5·45	7·73	0·703364	0·703365	2	0·512756	0·512783	2	n.d.	n.d.		n.d.	n.d.		n.d.	n.d.	
Tz Ca1	Tamazzart	−3·94	9·02	0·703460	0·703460	3	0·512757	0·512780	2	n.d.	n.d.		n.d.	n.d.		n.d.	n.d.	
Tz Ca5	Tamazzart	−5·09	7·83	0·703424	0·703424	3	0·512759	0·512785	3	19·068	19·132	0·000	15·528	15·565	0·001	38·825	39·036	0·001
Is Ca1	Issali-Igban	−5·81	7·46	0·703193	0·703193	3	0·512772	0·512790	2	19·420	19·464	0·004	15·548	15·584	0·003	39·046	39·238	0·008
Tz Ca4	Tamazzart	−4·84	8·36	0·703359	0·703359	2	0·512734	0·512757	3	19·097	19·187	0·002	15·539	15·577	0·002	38·858	39·024	0·004
Ts Ca1	Tisslit	−5·33	7·83	0·703168	0·703168	2	0·512790	0·512810	3	19·339	19·389	0·001	15·548	15·585	0·001	38·968	39·159	0·002
Tz Ca7	Tamazzart	−5·55	7·92	0·703386	0·703386	2	0·512718	0·512745	2	19·016	19·136	0·001	15·529	15·569	0·001	38·817	39·029	0·002
CMeA	Achakhchakh	−5·62	6·94	0·703435	0·703435	2	0·512740	0·512756	2	19·572	19·608	0·002	15·583	15·619	0·002	39·347	39·512	0·005
Tz Ca3	Tamazzart	−2·98	8·23	0·703617	0·703620	4	0·512747	0·512782	2	19·008	19·158	0·002	15·538	15·580	0·002	38·739	39·708	0·004
Tz Ca6	Tamazzart	−4·73	8·30	n.d.	n.d.		n.d.	n.d.		n.d.	n.d.		n.d.	n.d.		n.d.	n.d.	
Magnesiocarbonatites																		
Is Mg2	Issali-Igban	−0·26	17·36	0·703378	0·703378	3	0·51277	0·512796	3	19·851	19·917	0·003	15·587	15·624	0·002	39·218	39·938	0·006
Is Mg1	Issali-Igban	−1·14	13·82	0·703296	0·703296	2	0·512789	0·512803	3	19·777	19·917	0·003	15·579	15·620	0·002	39·320	39·698	0·005
Silicocarbonatites																		
Is Si1	Issali-Igban	−1·56	12·62	n.d.	n.d.		n.d.	n.d.		n.d.	n.d.		n.d.	n.d.		n.d.	n.d.	
Is Si2	Issali-Igban	−2·06	10·94	0·703239	0·703240	2	0·512812	0·512835	3	19·868	19·930	0·001	15·600	15·637	0·001	39·382	39·719	0·002
Ts Si	Tisslit	−2·26	10·08	0·703376	0·703472	3	0·512799	0·512824	2	19·784	19·846	0·003	15·573	15·611	0·002	39·381	39·718	0·006

*n.d., not determined.

to coarse-grained (sövites), essentially composed of calcite (80–90%), with variable amounts of fluorapatite (10–20%), pyrochlore (5–10%), and titanite (up to 10%) accompanied by minor green phlogopite (<800 μm), dolomite, ankerite, albite, K-feldspar and quartz (Fig. 2). The proportion of non-carbonate minerals, usually forming fine-grained interstitial intergrowths with carbonates, varies greatly among the veins and within single bodies.

Calcite occurs as euhedral to anhedral grains ~0·2–0·4 mm across, locally with a few calcite phenocrysts containing inclusions of celestine (up to 40 μm in length), bastnäsite-(Ce) (up to 20 μm across) and strontianite (<10 μm across). Coarse calcite grains, commonly up to 7 mm long and polysynthetically twinned, are highly interlocked, producing a mosaic texture with triple junctions, indicating equilibration under sub-solidus conditions. Where bordered by fine-grained calcite, the large calcite crystals invariably have serrated margins. Fluorapatite is abundant (locally up to 20 modal %) and forms round, elongated, purplish-blue cathodoluminescence colored grains and prisms (up to 0·4 and 1·0 mm), commonly poikilitically enclosed by either calcite or silicate phases (Fig. 2). Pyrochlore is exclusively restricted to the Tamazzart area (western Tamazert) calciocarbonatites and occurs either as small homogeneous grains included in calcite-host minerals or as large zoned light green to brown flaky crystals exhibiting alternating bands of different colors (Fig. 2). Cores of crystals are commonly dark and mantled by thin colorless zones, which in turn are surrounded by thick yellow margins. In contrast to pyrochlore, titanite occurs exclusively within the calciocarbonatites of the Issali-Igban and Tisslit areas (eastern Tamazert) as euhedral crystals up to several centimeters long (Fig. 2). Phlogopite forms subhedral homogeneous microphenocrysts to euhedral large zoned crystals up to 1 cm in diameter (Fig. 2).

Magnesiocarbonatites are restricted to the Issali-Igban and Tisslit areas (Fig. 1), where they crop out both as intrusive and extrusive bodies (diatremes). Intrusive magnesiocarbonatites occur either as meter-sized plugs or NW–SE-trending subvertical, 1–3 m thick, <100 m length along strike, dykes cutting across the nepheline syenites, the calciocarbonatites, and the diatreme structures. Altogether, intrusive magnesiocarbonatite occurrences make up *c.* 20% of the Tamazert carbonatite's volume.

In thin section, intrusive magnesiocarbonatites (beforsites) exhibit fine- (<50 μm) to medium-grained (1–5 mm) massive textures. They consist of >50% dolomite, up to 10% calcite and phlogopite. Dolomite, commonly untwinned, forms large euhedral to subhedral crystals with straight boundaries and frequent triple-junction intersections similar to those described in carbonatites elsewhere (Le Bas & Srivastava, 1989). No signs of corrosion of the euhedral calcite rhombs were noted. Some calcite phenocrysts have apparent 'overgrowths' of dolomite. These textural relationships are not consistent with replacement but are reminiscent of the phenocryst–groundmass relationships common in silicate igneous rocks (Harmer & Gittins, 1997). Euhedral to subhedral phlogopite shows frequent embayment. Non-carbonate constituents are apatite, magnetite and amphibole. They account for 1–5% of the rocks, are not uniformly distributed and usually form fine-grained interstitial intergrowths with carbonate.

Explosive magnesiocarbonatites occur exclusively within the Issali-Igban and Tisslit areas as steeply dipping diatreme structures filled with pyroclastic materials (including blocks of calciocarbonatite and remanent dykes of magnesiocarbonatite) and country rock xenoliths. The pyroclastic rocks consist of polymict tuffs, ash tuffs, lapilli tuffs and tuffisites (Stoppa & Lupini, 1993; Mourtada, 1997), accompanied by polygenetic volcaniclastic breccias. The lithic fragments include clasts of the surrounding country rocks (marble, pyroxenites, lamprophyres, foidsyenites and sedimentary carbonate wall-rocks). In thin section, representative extrusive magnesiocarbonatite samples show megascopic breccia-like textures, consisting of crust and mantle fragments accompanied by poorly sorted globular lapilli set in a brown-weathered, fine-grained groundmass mosaic of ferroan dolomite. Compound lapilli are abundant, containing aggregates of up to 1·5 mm in diameter spherical globules cemented by drusy calcite or supported by an ash iron-rich dolomitic matrix. Globules consist of iron-bearing dolomite with small amounts of biotite. In some compound lapilli, there are concentric zones of more carbonate-rich material (beforsite) grading outward to a feldspar and oxide-rich cortex (Mourtada, 1997). Single dolomite crystals are rimmed by Fe-rich carbonate overgrowths. Primary textures are not well preserved and all of the diatreme-type structures have undergone significant chemical changes during a period of hydrothermal alteration.

Mineralogically, the extrusive magnesiocarbonatites consist of >70% Fe-rich dolomite grains and laths (100–300 μm) accompanied by microphenocrysts (950–150 μm) of fluorapatite and phlogopite. Interstices may be filled with late-stage hydrothermal quartz, albite, K-feldspar, barite, strontianite, purple fluorite, and/or REE-bearing fluorocarbonates (parisite-synchisite) and sulfides (pyrite, sphalerite and galena).

Silicocarbonatites are most commonly associated with occurrences of magnesiocarbonatite, although some are related to melteigite rocks and occur as white, coarse-grained intercumulus-textured calcite, filling the interstices between clinopyroxene (250–800 μm), schorlomite garnet (up to 1 mm) and phlogopite (up to 3 cm) (Fig. 2). Silicocarbonatites contain mostly ankerite and ferroan-dolomite with minor calcite and dolomite. Biotite is also

present, reflecting a higher Fe content. Apatite forms stubby grains, commonly poikilitically enclosed by either calcite or silicate phases. Other accessory phases include fluorite, barite and sulfides.

Mineral chemistry

Microprobe analyses show that the Tamazert carbonate compositions vary from pure calcite to dolomite to ankeritic dolomite and ultimately ankerite. Regardless of grain size, calcite has a Sr content (0·3–0·9 wt % $SrCO_3$) comparable with that of carbonatites worldwide (SrO = 0·2–1·4 wt %; Hornig-Kjarsgaard, 1998). The average contents of $FeCO_3$, $MgCO_3$, MnO_3 and BaO are relatively low, varying in the range of 0·2–1 wt %, 0·1–0·2 wt %, 0·1–2 wt %, and 0–0·1 wt %, respectively (Table 2).

CaO and FeO are also major components in dolomite, reflecting a large range in Ca/(Ca + Mg + Fe) ratios; minor elements such as SrO and MnO also show a wide variation (Table 2). Ankerite yields $CaCO_3$, $FeCO_3$, $MgCO_3$ and MnO_3 values in the range of 48·5–52 wt %, 16·3–24·7 wt %, 23·4–29·1 wt % and 1·5–4·9 wt %, respectively. The contents of $Ba(CO_3)$ are very low. All the analyzed carbonate minerals have very low La_2O_3 and Ce_2O_3 contents, mostly below detection limits (Table 2). The application of the dolomite–calcite geothermometer of Anovitz & Essene (1987) indicated that the Tamazert carbonate rocks equilibrated at various temperatures, ranging from 430–700°C for sövites to 254–279°C for alvikites (Mourtada, 1997).

Apatite shows little variation in chemistry and approaches the idealized formula $Ca_5(PO_4)_3(F, OH, Cl)$. Compositionally, apatite is characterized by LREE enrichment ($\sum LREE_2O_3 = 0{\cdot}05$–$1{\cdot}16$ wt %, with $Ce_2O_3 > La_2O_3$) and low Mn (<0·04 wt % respective oxides), and corresponds to fluorapatite with F concentrations ranging from 4·2 to 7·5 wt %, similar to apatite crystals occurring worldwide in carbonatites (Hogarth, 1989). The Na_2O content is about 0·5 wt % indicating the usual coupled REE–Na substitution. Representative compositions of apatite are listed in Table 2. Compared with the composition of apatite from the calciocarbonatites of the Issali-Igban and Tisslit areas, apatite crystals in the Tamazzart calciocarbonatites are enriched in F (average 5·54 wt % against 4·75 wt %), and particularly in Ce_2O_3 (average 0·47 wt % against 0·09 wt %) and are relatively depleted in CaO (53 wt % against 54·5 wt %).

Pyrochlore displays a composition close to the theoretical formula $(Ca, Na)_2(Nb, Ti, Ta)_2O_6(OH, F, O)$ (Table 2). The analyzed crystals are relatively Ca-rich (rather than Na-rich) and Ca contents tend to decrease from the core (15·4–16·3 wt %) to the edge (14·2–15 wt %) of the crystals. The small homogeneous pyrochlore grains are LREE-rich ($\sum La_2O_3 + Ce_2O_3 + Nd_2O_3 = 787$–$45$ ppm). Na_2O scatters between 3·1 and 7·4 wt %, ZrO_2 between 0·3 and 1·7 wt %, and F between 2·3 and 5·3 wt % (Table 2). In general, the pyrochlore has high Nb concentrations (57–63·5 wt % Nb_2O_5), partly replaced on site B by Ti (6–7·3 wt % TiO_2) and Ta (0–0·2 wt % Ta_2O_5).

Titanite displays uniform compositions with SiO_2, TiO_2, CaO and FeO contents in the range of 30·1–30·7 wt %, 34·3–34·8 wt %, 27·6–27·9 wt %, and 1·8–1·9 wt %; respectively (Table 2).

Phlogopite covers a somewhat wider range of compositions, with SiO_2, MgO, TiO_2, FeO and F concentrations in the range of 38–43·7 wt %, 14·8–25·4 wt %, 0·2–2·78 wt %, 3·51–16·5 wt % and 0·21–6·83 wt %; respectively. The K_2O contents are relatively uniform, varying in a restricted interval from 9·14 to 10·6 wt %, whereas the BaO contents are very low (<0·2 wt %). Based on its thin-section pleochroic colour, two types of phlogopite are recognized, varying from reddish brown to green. They are also distinguishable by their compositions: ferriphlogopite and green fluorphlogopite (Table 2). Fluorphlogopite, characterized by its F content averaging 5·47 wt %, occurs in the calciocarbonatites of the Issali Ighban area, whereas ferriphlogopite, more depleted in F with concentrations averaging 0·97 wt %, is limited to the Tisslit and Oued Tamazzart areas (Fig. 1).

Locally, feldspars constitute a modally significant constituent of the Tamazert calciocarbonatites (Table 2), albite (An ≤ 2) and two-feldspar intergrowths.

GEOCHEMISTRY

Whole-rock major and trace element compositions

As expected from their mineralogy, the major element geochemistry of the carbonatites shows a large range in CaO (2–57 wt %), MgO (0·1–19 wt %) and SiO_2 (1·2–30·8 wt %) contents, allowing the classification of the Tamazert carbonatites into three groups (Fig. 3): (1) calciocarbonatites with CaO > 47 wt %, MgO < 1 wt % and SiO_2 < 7 wt % (sövites, microsövites and alvikites depending on their grain-size); (2) magnesiocarbonatites with CaO < 35 wt %, MgO > 18 wt % and SiO_2 < 7 wt % (beforsites and tuffisites); (3) silicocarbonatites with CaO < 25 wt %, MgO < 10 wt % and SiO_2 > 19 wt %, and Fe_2O_3 and Al_2O_3 contents in the range of 0·2–7·7 wt % and 0·3–5·5 wt %, respectively. Compared with calciocarbonatites, magnesiocarbonatites are slightly enriched in Fe_2O_3 (3·42–5·73 wt %; average 0·9 wt % and 0·2–3·58 wt %; average 4·6 wt %). The compositions of the calcio- and magnesiocarbonatites are comparable with those reported previously (Agchmi, 1984; Mourtada, 1997). The silicocarbonatites have the highest Fe_2O_3 and Al_2O_3 contents, reflected in the presence of ferroan-dolomite and ferroan-calcite. The silicocarbonatites are not true carbonatites as their carbonate contents are too low (e.g. <50 modal %) (Le Maitre, 2002), but the term

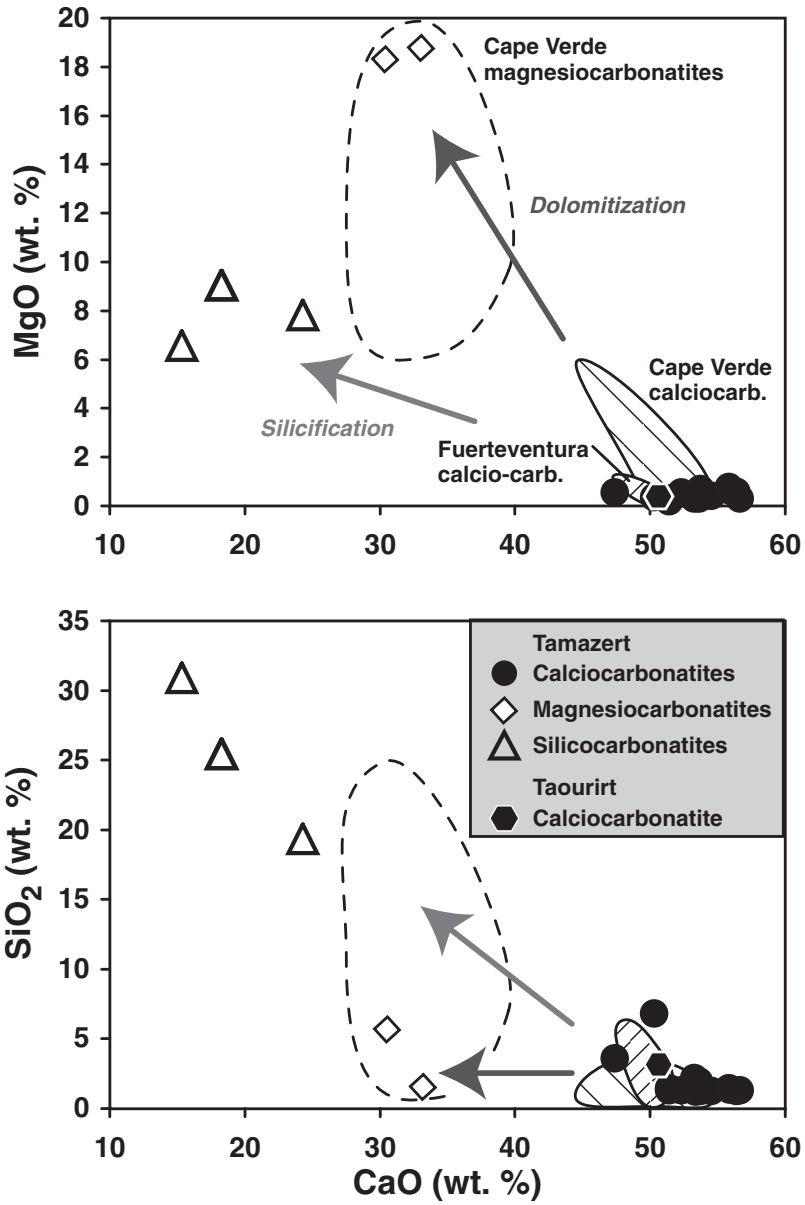

Fig. 3. Major element composition of the calcio-, magnesio- and silicocarbonatites from Tamazert and a calciocarbonatite xenolith from the nearby Taourirt area (xenolith in lamprophyre), as well as the oceanic Cape Verde and Canary (Fuerteventura) Islands. Data sources: carbonatite xenolith from Taourirt from Wagner *et al.* (2003); carbonatites from the Cape Verde and Canary Archipelagos from Hoernle & Tilton (1991) and Hoernle *et al.* (2002).

'silicocarbonatites' is used below for convenience. Based on thin-section petrography, the high SiO_2 content of the silicocarbonatites is secondary in origin as a result of the abundance of K-feldspar and hydrothermal quartz along with biotite, barite, strontianite, fluorite and sulfides.

The carbonatites show large variations in the abundances of most trace elements (Fig. 4, Table 3). Large ion lithophile elements (LILE), such as Cs, Rb, Ba, K, Pb, Sr and Li, REE and high field strength elements (HFSE), such as the Nb, Ta, Ti, Zr and Hf, range from well below primitive mantle values to values >4000 times above (Fig. 4). The HFSE contents of the magnesiocarbonatites are similar to those of the calciocarbonatites and their distribution shows no evolutionary trend as outlined by Chakhmouradian (2006). The Sr concentrations of the calciocarbonatites are extremely high (1131–36 260 ppm), overlapping those of magnesio- and silicocarbonatites (1088–17 017 ppm). La concentrations range from 2·7 to

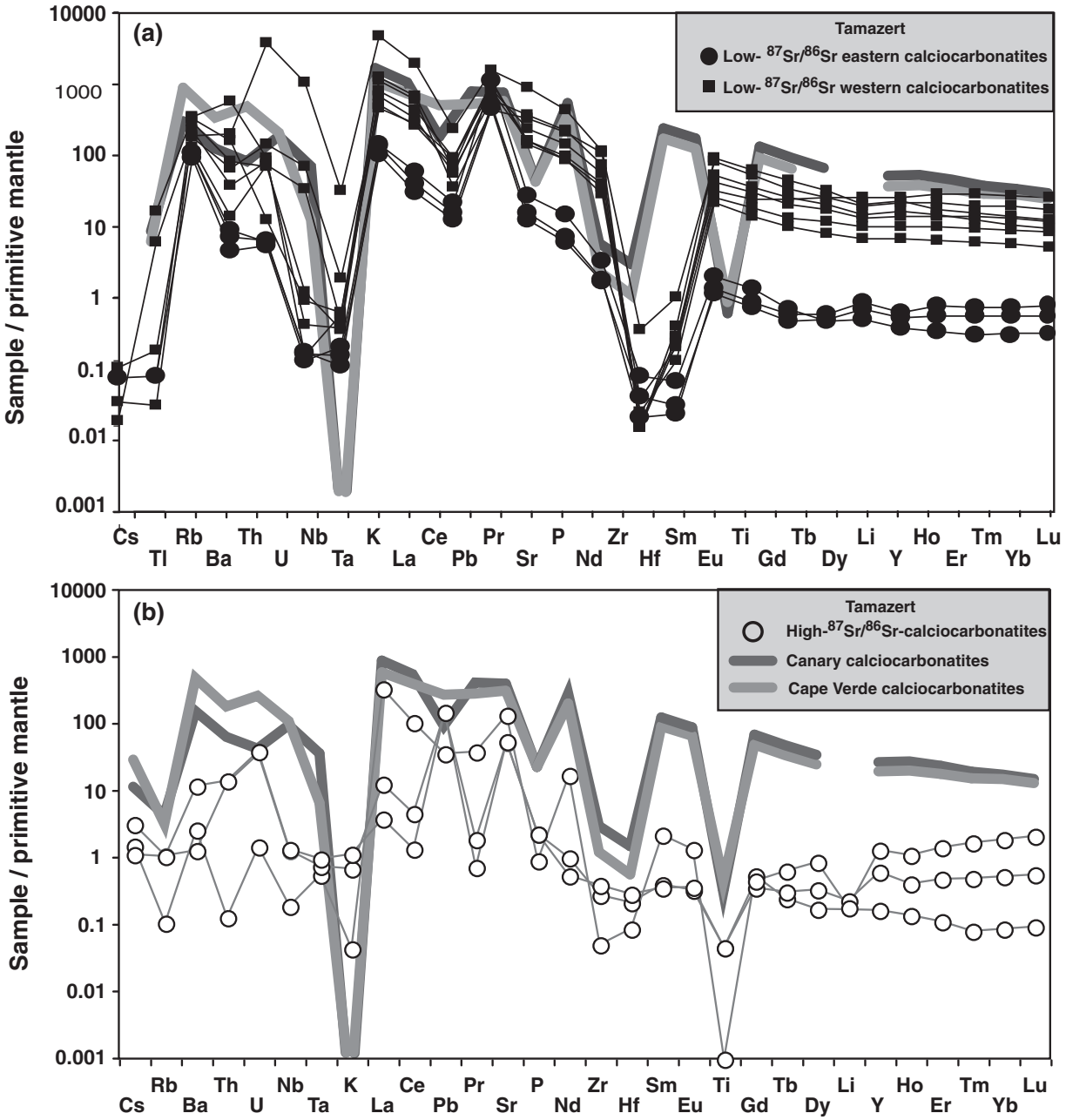

Fig. 4. Multi-element diagrams showing primitive mantle-normalized trace element concentrations of Tamazert low-$^{87}Sr/^{86}Sr$ (a) and high-$^{87}Sr/^{86}Sr$ (b) calciocarbonatites and Tamazert magnesio- (c) and silicocarbonatites (d), compared with calcio- and magnesiocarbonatites from the Cape Verde and Canary Islands. Data sources: Cape Verde and Canary Islands carbonatites from Hoernle & Tilton (1991) and Hoernle *et al.* (2002); primitive mantle from Sun & McDonough (1989).

3·4 ppm. Cr and Ni concentrations are very low and close to the detection limits of both X-ray fluorescence (XRF) and ICP-MS for the calciocarbonatites (<2·4 ppm), moderate for the magnesiocarbonatites (2·7–46·2 ppm) and elevated for the silicocarbonatites (170–393 ppm). The carbonatites also show large ranges in the ratios of trace elements, which are similar to those found in relatively primitive basaltic liquids, such as Ba/Th (7–1680), U/Th (0·3–38·3), Nb/Ta (5–752), K/La (0–109), La/Yb (3–5400), Pb/Nd (0·03–14·53), Sr/Nd (7·0–1·6) and Zr/Hf (2–84). The large variation in highly incompatible element concentrations and trace element ratios reflects the presence of exotic mineral phases that carry large amounts of these generally incompatible elements, such as pyrochlore

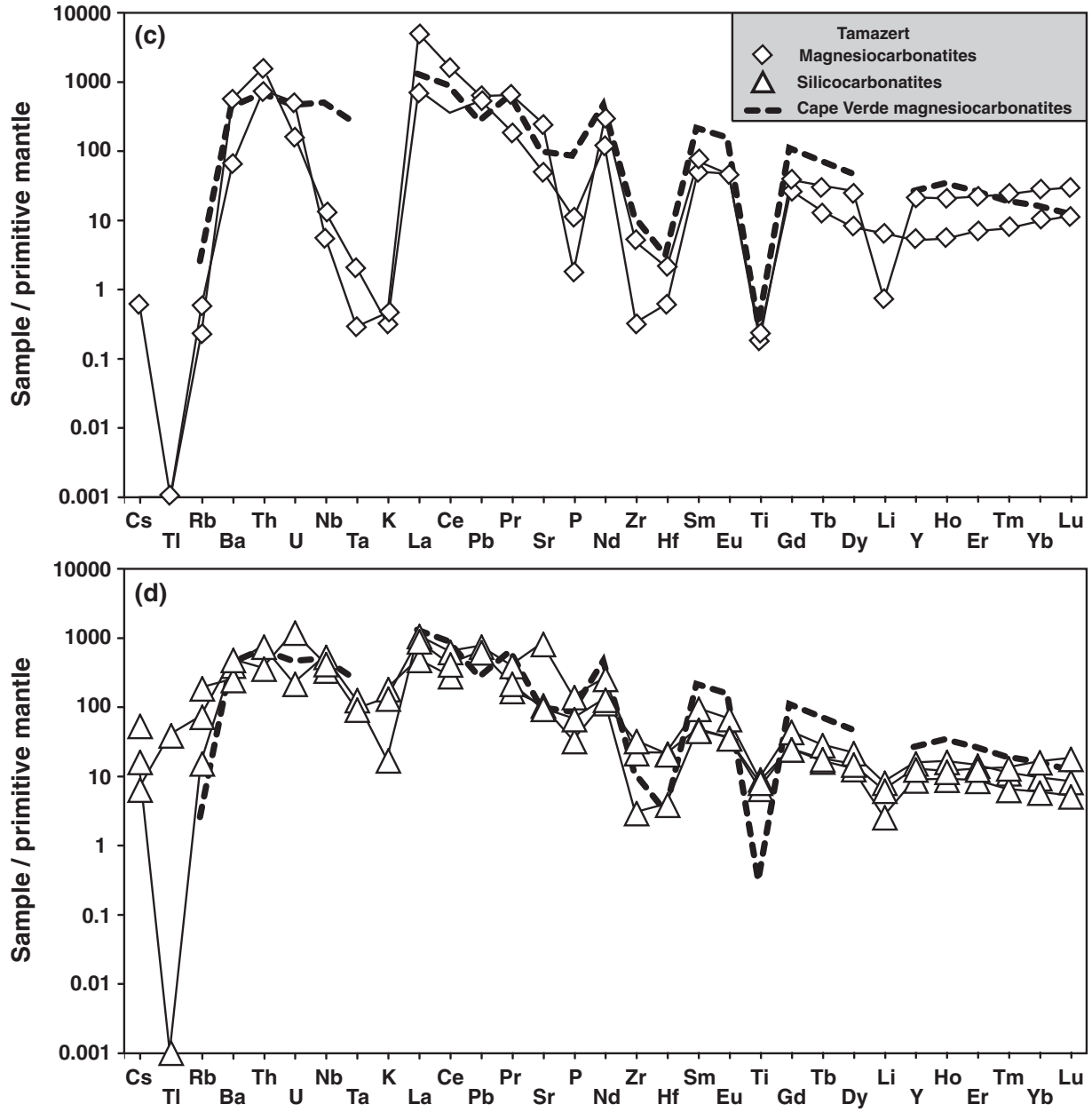

Fig. 4. Continued.

(HFSE and LREE), titanite (Ti and other HFSE), apatite (LREE, Sr, U, Th) and biotite (K, Rb). Two of the eastern Tamazert calciocarbonatites (samples ISCa2 and IsCa3) have very low LREE and HFSE and very high Pb/Nd ratios (up to 14·5), which could in part be explained by the fractionation of pyrochlore.

The primitive mantle-normalized incompatible element patterns of the Tamazert carbonatites generally show troughs at K, P, Zr, Hf, Ti, Li, Ta and Nb coupled with relative enrichment of Sr, Th, U, Pb and the LREE. Most calciocarbonatites show incompatible element patterns very similar to those of calciocarbonatites from the Canary and Cape Verde Islands (Hoernle & Tilton, 1991; Hoernle *et al.*, 2002) (Fig. 4a and b). The six calciocarbonatites from the eastern Tamazert complex (Tisslit and Issali-Igban areas) have lower REE concentrations, including three samples from calciocarbonatites intruding Jurassic limestones, than the western Tamazert calciocarbonatites from Tamazzart (Fig. 4a and b). The limestone-hosted calciocarbonatites are also distinguished by their

low Sr and Ba concentrations, reduced or lacking negative P-, Zr-, Hf- and Li-anomalies and a relative enrichment of the LREE and HREE compared with the middle REE (MREE) in two samples, resulting in U-shaped REE patterns. The magnesiocarbonatites have much higher Th and much lower Sr than the calciocarbonatites. V, Cr, Co and Ni are also higher in the magnesiocarbonatites. Moreover, the REE and trace element patterns of the magnesiocarbonatites are similar to those of magnesiocarbonatites from the Cape Verde Islands (Fig. 4c). Mantle-normalized incompatible element patterns for the silicocarbonatites are similar to those of the calcio- and magnesiocarbonatites, with the exception of reduced or lacking negative HFSE, K and Li anomalies (Fig. 4d).

C–O isotopic compositions

The C and O isotope data for various types of carbonatites from the Tamazert complex are summarized in Table 4 and plotted in Fig. 5a. Altogether, the analyzed carbonatite samples display large variations in $\delta^{13}C$ and $\delta^{18}O$, ranging from −5·8 to +1·7‰, and +6·9 to +23·5‰, respectively. The most striking feature is that there are significant variations in the $\delta^{13}C$ and $\delta^{18}O$ values depending both on the carbonatite type (calcio-, magnesio- and silicocarbonatites) and the petrographic composition of the host-rock. Calciocarbonatites cutting across nepheline syenites (*s.l.*) tend to have the lowest $\delta^{13}C$ (−5·8 to −3·9‰) and $\delta^{18}O$ (6·9–9·0‰) and plot within or close to the 'primary igneous carbonate' mantle box of Taylor *et al.* (1967), Deines & Gold (1973) and Keller & Hoefs (1995). In contrast, calciocarbonatites cross-cutting the Liassic limestones (e.g. samples IsCa1 and IsCa3) have the highest $\delta^{13}C$ and $\delta^{18}O$ (up to +1·7‰ and +23·5‰, respectively). The magnesio- and silicocarbonatites commonly have higher $\delta^{13}C$ (−1·1 to −0·3‰ and −2·3 to −1·6‰) and $\delta^{18}O$ (+13·8 to + 17·4‰ and + 10·1 to + 12·6‰) values than most of the calciocarbonatites. In the C–O isotope diagram (Fig. 5a), the Tamazert carbonatites form an array between the mantle box and marine sediments.

Sr–Nd–Pb isotopic composition

Initial Sr–Nd–Pb isotope ratios were calculated using an average formation age of 40 Ma inferred from the available K–Ar and Rb/Sr systematics (Tisserant *et al.*, 1976). The whole-rock isotopic analyses of the carbonatites yield a restricted range in $^{143}Nd/^{144}Nd$ values varying between 0·51254 and 0·51282, but show a wider range in $^{87}Sr/^{86}Sr$ ratios (0·7031–0·7076), similar to the published data for three carbonatite samples from Tamazert and the Taourirt area *c.* 300 km NE of the Tamazert complex (Bernard-Griffiths *et al.*, 1991; Wagner *et al.*, 2003). Most Tamazert carbonatites form an array together with those from the Canary and Cape Verde Islands, but trend towards lower $^{143}Nd/^{144}Nd$ (Fig. 5b). The Tamazert calciocarbonatites can be divided into two groups based on their Sr and Nd isotopic compositions: (1) calciocarbonatites with relatively low $^{87}Sr/^{86}Sr$ (<0·7040) but elevated $^{143}Nd/^{144}Nd$ (>0·5127) that fall on the Canary–Cape Verde array; (2) those with high $^{87}Sr/^{86}Sr$ (>0·7040) and low $^{143}Nd/^{144}Nd$ (<0·5127) that do not fall on the Canary–Cape Verde array. Notably, the high-$^{87}Sr/^{86}Sr$ calciocarbonatites intruded into Liassic limestones. Two of these samples also have the highest $\delta^{13}C$ and $\delta^{18}O$ of all carbonatites (Fig. 5a). Sr and Nd isotope ratios of the magnesio- and silicocarbonatites are nearly indistinguishable from those of the low-$^{87}Sr/^{86}Sr$ calciocarbonatites, except that the silicocarbonatites extend to slightly higher Nd isotope ratios, and they overlap the field of the Cape Verde calciocarbonatites (Fig. 5b).

The initial Pb isotope ratios of the analyzed carbonatites show significant variations: $^{206}Pb/^{204}Pb = 18·29–19·89$, $^{207}Pb/^{204}Pb = 15·56–15·64$ and $^{208}Pb/^{204}Pb = 38·24–39·55$. The calciocarbonatites from western Tamazert have lower $^{207}Pb/^{204}Pb$ isotope ratios than calciocarbonatite samples from eastern Tamazert. On the uranogenic Pb isotope diagram (Fig. 6a), the low-$^{87}Sr/^{86}Sr$ calciocarbonatites from western and eastern Tamazert plot along the Northern Hemisphere Reference Line (NHRL). In contrast, the high-$^{87}Sr/^{86}Sr$ calciocarbonatites from eastern Tamazert plot above (to the left of) the NHRL on the urano- and thorogenic Pb isotope diagrams and form an array towards a low-$^{206}Pb/^{204}Pb$ component with positive $\Delta 7/4$ and $\Delta 8/4$. The magnesio- and silicocarbonatites have slightly higher $^{206}Pb/^{204}Pb$ ratios than the calciocarbonatites, which is the opposite of what is observed for calcio- and magnesiocarbonatites from the Cape Verde Islands (Fig. 6) (Hoernle *et al.* 2002). The Tamazert magnesio- and silicocarbonatites fall below the NHRL on both Pb isotope diagrams and overlap the field for the Cape Verde calciocarbonatites on the uranogenic Pb isotope diagram; they fall between the Cape Verde and Canary calciocarbonatites on the thorogenic Pb isotope diagram. In summary, despite their high C and O isotope values, the magnesio- and silicocarbonatites have Sr–Nd–Pb isotope ratios similar to the Cape Verde and Canary calciocarbonatites, which in turn have mantle-type C and O isotope values.

DISCUSSION

Late-stage sub-solidus and crustal processes

Because field and thin-section observations indicate that the Tamazert carbonatites have fenitized the surrounding silicate rocks, the primary carbonatite magma is likely to have been alkaline, consistent with experimental data (Wallace & Green, 1988; Sweeney, 1994; Yaxley & Green, 1996). Keppler (2003) showed that the decrease at low pressures of water solubility in carbonatitic melts results in the expulsion of fluids and thus hydrothermal alteration

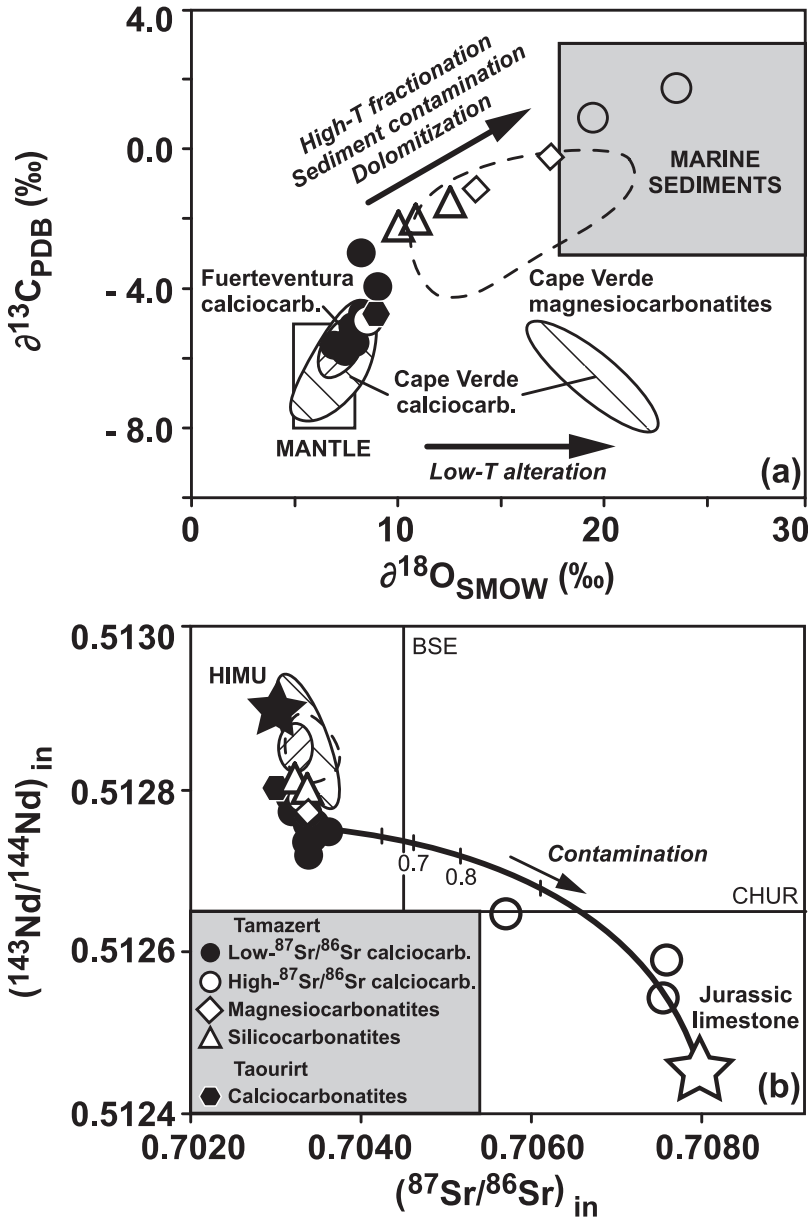

Fig. 5. C–O isotope (a) and Sr–Nd isotope (b) composition of continental Tamazert carbonatites, compared with a carbonatite xenolith from Taourirt and carbonatites from the Cape Verde and Canary Islands. The hyperbola in (b) indicates mixing between a low-$^{87}Sr/^{86}Sr$ calciocarbonatite and Jurassic limestone. Numbers along the hyperbola indicate the mixing parameter *f*. Mixing parameters for the calciocarbonatite and limestone are, respectively: 2500 ppm and 1000 ppm for Sr concentrations, 70 ppm and 2 ppm for Nd concentrations, 0·703349 and 0·708000 for Sr isotope ratios, and 0·512755 and 0·512450 for Nd isotope ratios. Data sources: Jurassic limestone from Bouabdli *et al.* (1988); Taourirt carbonatite xenolith from Wagner *et al.* (2003); Cape Verde and Canary Islands carbonatites from Hoernle & Tilton (1991) and Hoernle *et al.* (2002); mantle and marine sediment boxes for carbonatites from Taylor *et al.* (1967) and Keller & Hoefs (1995); HIMU, BSE and CHUR from Zindler & Hart (1986).

(e.g. fenitization) of the surrounding wall-rocks. The effects of such alteration are much stronger around shallow carbonatite complexes, as a result of the greater amount of hydrous fluid expulsion, than around deep intrusions. An estimated depth of <3 km for the emplacement of the Tamazert intrusion is consistent with the strong fenitization observed around the intrusive complex (Salvi *et al.*, 2000; Marks *et al.*, 2008). In addition to the development of fenites, the Tamazert carbonatites experienced the effects of an extensive late- to post-magmatic alteration event, as shown by the development of the widespread hydrothermal mineral paragenesis of fluorite, barite,

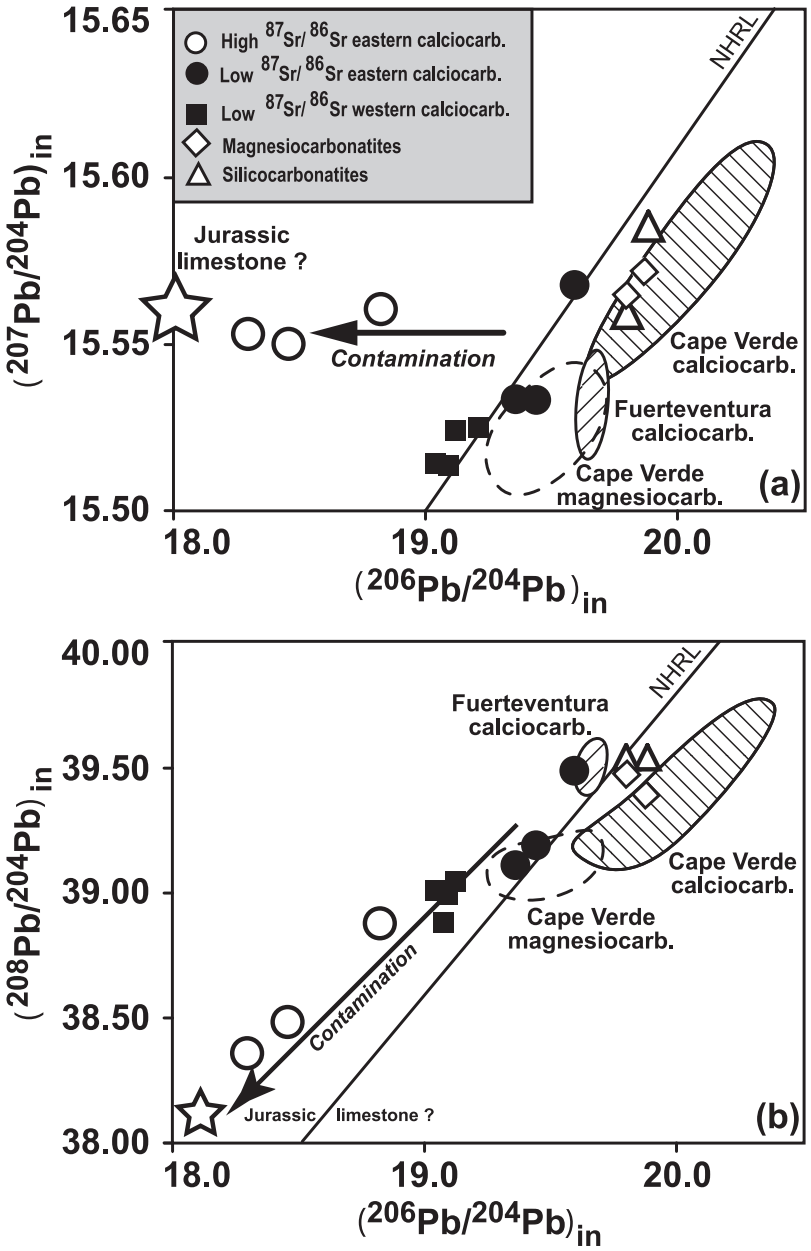

Fig. 6. Pb isotopic composition of carbonatites from the continental Tamazert igneous complex and the oceanic Cape Verde and Canary Islands. Data sources: Cape Verde and Canary Islands carbonatites from Hoernle & Tilton (1991) and Hoernle *et al.* (2002); Northern Hemisphere Reference Line (NHRL) from Hart (1984). (a) $^{207}Pb/^{204}Pb_i$ vs $^{206}Pb/^{204}Pb_i$; (b) $^{208}Pb/^{204}Pb_i$ vs $^{206}Pb/^{204}Pb_i$.

strontianite, celestine and REE carbonates within the carbonatites. The existence of fluorite suggests the involvement of an F-rich hydrothermal fluid derived from the carbonatite itself. Carbonatites also release fluids rich in Ca, Sr, Mn, REE, HFSE and CO_2 (e.g. Woolley, 1982; Platt & Woolley, 1990; Bühn, 2008; Schilling *et al.*, 2009); these appear to have affected both the surrounding host-rocks and parts of earlier emplaced carbonatites.

Although most of the calciocarbonatites show a relatively restricted range in chemical composition, three of the analyzed samples have much more radiogenic $^{87}Sr/^{86}Sr$ and less radiogenic $^{143}Nd/^{144}Nd$ and $^{206}Pb/^{204}Pb$ isotopic compositions than the other calciocarbonatites. It is commonly assumed that the Sr and Nd isotopic composition of carbonatites cannot be changed by alteration processes, as a result of their high Sr and Nd concentrations. Interestingly, the three samples with anomalous radiogenic isotopic compositions also have low Sr (1130–2860 ppm compared with 12 000–36 000 ppm for other calciocarbonatites) and Ba contents (9–84 ppm vs 1000–3400 ppm).

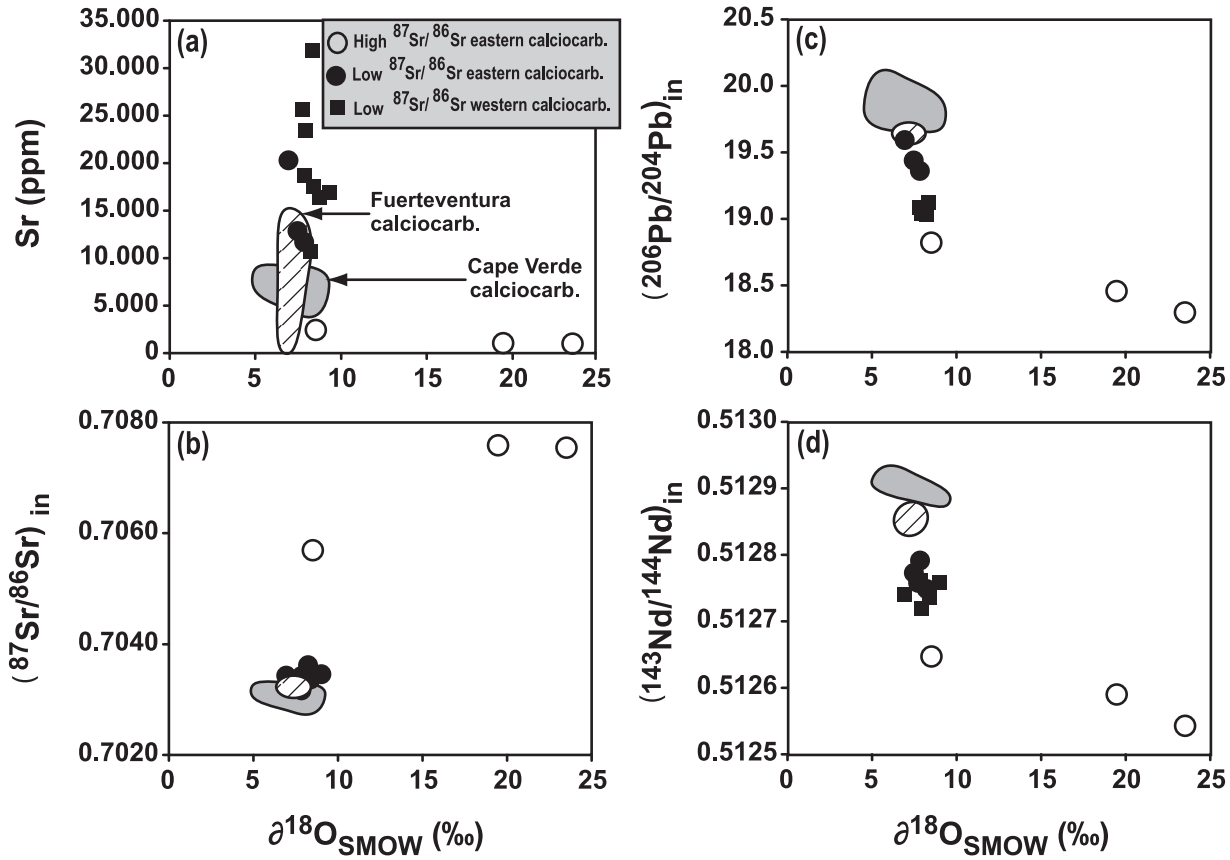

Fig. 7. Variation of (a) Sr (ppm), (b) $(^{87}Sr/^{86}Sr)_i$, (c) $(^{206}Pb/^{204}Pb)_i$ and (d) $(^{143}Nd/^{144}Nd)_i$ vs $\delta^{18}O_{SMOW}$ for Tamazert continental calciocarbonatites compared with oceanic calcicarbonatites from Cape Verde and Fuerteventura islands. It should be noted that calciocarbonatites from eastern Tamazert that have elevated $\delta^{18}O$ also have: (a) low Sr concentrations, (b) radiogenic Sr and (c, d) unradiogenic Pb and Nd isotope ratios, respectively. Data sources: Cape Verde and Canary Islands (Fuerteventura) carbonatites from Hoernle & Tilton (1991) and Hoernle *et al.* (2002).

Cathodoluminescence microscopy shows that some calcite crystals have a Sr-rich core, mantled by a secondary low-Sr rim, indicating that the low Sr concentrations are not a primary but a late-stage feature of the carbonatites. The lower $^{206}Pb/^{204}Pb$ and $^{208}Pb/^{204}Pb$ isotope ratios of these three calciocarbonatite samples (Fig. 6) also suggest a significant input of upper crustal Pb (Zartman & Doe, 1981) during ascent of the carbonatitic magma.

The three samples with anomalous Sr, Nd and Pb isotopic compositions also have elevated O and C isotopic compositions compared with mantle values (Figs 5a and 7b–d). The elevated stable isotopic compositions can result from: (1) crustal contamination involving assimilation of sedimentary wall-rocks during magma emplacement (Anderson, 1987); (2) high-temperature fractionation within a carbonatite magma (Deines, 1989); (3) loss of isotopically light water during pressure reduction (Deines & Gold, 1973); (4) equilibration of carbonates with meteoric water (at a temperature of <250°C) (Coulson *et al.*, 2003). Because the radiogenic isotopes are also anomalous, crustal contamination is the most likely explanation for the elevated O and C isotopic values.

Limestones have low Sr and Ba concentrations and high $\delta^{18}O$ and $\delta^{13}C$ values compared with mantle-derived carbonatite melts, radiogenic $^{87}Sr/^{86}Sr$ (reflecting that of seawater when the limestone formed), and Nd and Pb isotopic compositions that are likely to reflect the composition of local Jurassic pelagic sediments (i.e. unradiogenic $^{143}Nd/^{144}Nd$ and $^{206}Pb/^{204}Pb$, and $^{207}Pb/^{204}Pb$ and $^{208}Pb/^{204}Pb$ well above the NHRL for a given $^{206}Pb/^{204}Pb$). Therefore mixing of the Jurassic limestone that hosts the Tamazert complex with the calciocarbonatite magma could explain the anomalous composition of the three calciocarbonaties. However, illustrated by the model mixing curve in Fig. 5b, addition of more than 85% of the host limestone to an average calciocarbonatite is necessary to explain the extremely radiogenic Sr and unradiogenic Nd isotopic composition of the three anomalous calciocarbonatites. Such large addition of limestone to the carbonatites is also consistent with the dilution of Sr and Ba

concentrations in these samples roughly by a factor of 10. The mantle-derived calciocarbonatite and/or related mantle-derived silicate melts are likely to have caused melting of the surrounding Jurassic carbonates and other crustal rocks, which may included sulfides rich in Pb. Mixing of the eastern Tamazert calciocarbonatite melts with >85% of the secondary limestone melts could generate the trace element and stable and radiogenic isotopic compositions observed in the low-Sr, high-$^{87}Sr/^{86}Sr$ calciocarbonatites from eastern Tamazert, consistent with the emplacement of these melts into the limestones. Alternatively, <15% addition of mantle-derived calciocarbonatite melt to the host limestone could also generate the observed chemical compositions. This scenario, however, is not consistent with the cross-cutting relationship between the high-$^{87}Sr/^{86}Sr$ calciocarbonatites and the host limestone.

As noted above, regional differences in geochemistry also exist between the calciocarbonatites. The calciocarbonatites from eastern Tamazert have lower REE, Y, Pb, U and Th abundances and higher Pb isotope ratios than those from western Tamazert, regardless of whether they have O and C isotope compositions plotting in the mantle range and low Sr concentrations and isotope ratios or extremely elevated O, C and Sr isotopic compositions (Figs 4 and 6a). Although these regional variations in trace element and isotopic composition do not correlate with indices of alteration or crustal interaction (e.g. O, C and Sr isotope ratios), extensive fractionation of phases such as apatite and sulfides could, in part, explain the differences in trace element composition compared with the calciocarbonatites from western Tamazert. The difference in Pb isotopic composition, however, cannot be explained by fractional crystallization or variations in the degree of melting, but must reflect differences in the composition of the sources (crustal and mantle) contributing to the sampled calciocarbonatites.

Magnesiocarbonatites, occurring mainly as porous breccias and permeable diatremes, show extensive recrystallization accompanied by the replacement of calcite with secondary dolomite, and the development of a secondary mineral paragenesis made of ankerite, fluorite, pyrochlore, apatite, barite, strontianite, celestine, sulfides and Fe-oxides. Replacement of calcite by dolomite, triggered by MgO-rich hydrothermal fluids, can explain the increase in MgO, $\delta^{13}C$ and $\delta^{18}O$ and decrease in CaO and Sr observed in the magnesiocarbonatites (Figs 3 and 5a). The Tamazert magnesiocarbonatites have trace element patterns similar to the high-REE calciocarbonatites from western Tamazert, except that Th is much higher and Sr much lower. On the other hand, the Sr, Nd, $^{207}Pb/^{204}Pb$ and $^{208}Pb/^{204}Pb$ isotope ratios of the magnesiocarbonatites are similar to those of the high-Sr calciocarbonatites from western Tamazert, but their $^{206}Pb/^{204}Pb$ ratios are slightly higher (Figs 5 and 6).

If the magnesiocarbonatites were ultimately produced by the recrystallization of calciocarbonatites similar to those from eastern Tamazert, the higher $^{206}Pb/^{204}Pb$ ratios of the magnesiocarbonatites in comparison with the calciocarbonatites could result from one of the following processes. (1) The dolomitic matrix was precipitated from fluids having a relatively high $^{206}Pb/^{204}Pb$ isotope ratio (e.g. derived from mafic and ultramafic igneous silicate rocks or melts in the complex). (2) U loss or Pb gain caused a decrease in the U/Pb ratio during the dolomitization process that occurred millions of years after the parental calciocarbonatites formed. This would have resulted in an undercorrection for radiogenic ingrowth using the measured U/Pb ratio. In other words, a higher U/Pb ratio is needed to correct the sample for radiogenic ingrowth during part of the time after its formation. (3) The Pb isotopic compositions reflect primary differences in the carbonatite magma sources.

If the basement silicate rocks providing the MgO for the magnesiocarbonatites were derived from the same source as the carbonatites, but had high U/Pb ratios, they could have evolved more radiogenic $^{206}Pb/^{204}Pb$ through time without significantly affecting the other isotope systems. The $^{207}Pb/^{204}Pb$ isotope ratios would not have been significantly affected, because of the low abundance of ^{235}U relative to ^{238}U (1/137·88) in the present-day Earth. The $^{208}Pb/^{204}Pb$ isotope ratios would also not have been affected, because ^{208}Pb is derived from the decay of ^{232}Th, which has a significantly longer half-life than ^{238}U. If these silicate rocks also provided the Pb for the magnesiocarbonaties, they could have caused an increase in $^{206}Pb/^{204}Pb$ without affecting the other isotopic systems. The lack of change in the Sr and Nd isotopic composition could reflect the following: (1) the fluids causing the dolomitization had low concentrations of Sr and Nd; (2) the dolomite did not incorporate Sr or Nd from the fluids, which is likely for Sr as it is less compatible in dolomite than in calcite and the Sr concentrations are much lower than in the calciocarbonatites, the presumed parents of the magnesiocarbonatites; (3) the Sr and Nd isotopic compositions of the rocks or melts from which the Pb was derived had similar Sr and Nd isotopic compositions. Alternatively, a regional hydrothermal event occurring millions of years after the emplacement of the calciocarbonatites that also caused the recrystallization of calciocarbonatites to magnesiocarbonatites (and possibly also the silicocarbonatites; see below) could also have decreased the U/Pb ratio. The magnesiocarbonatites, however, have higher U/Pb ratios (0·09–0·24) (and silicocarbonatites: U/Pb = 0·09-·57) than the spatially related eastern calciocarbonatites (0·01–0·08) and therefore this is not a viable possibility. Interestingly, the Cape Verde

magnesiocarbonatites also have distinct Pb isotopic compositions from the associated calciocarbonatites, but they have less radiogenic rather than more radiogenic Pb isotopic compositions. Hoernle *et al.* (2002), on the basis of the absence of a crustal endmember with an appropriate isotopic composition, concluded that the isotopic composition of the Cape Verde magnesiocarbonatites reflected that of their mantle source.

In summary, we interpret the geochemistry of the magnesiocarbonatites to reflect interaction, at crustal levels, with Mg-rich late-stage hydrous fluids that accompanied the emplacement of the carbonatites. The Mg in the fluids was certainly leached from mafic and ultramafic igneous rocks that also crop out in the area and belong to the Tamazert ijolite–syenite–carbonatite complex. The elevated $^{206}Pb/^{204}Pb$ isotope ratios of the magnesiocarbonatites, as compared with the calciocarbonatites from eastern Tamazert, may have been derived from such mafic and ultramafic igneous rocks or reflect a source characteristic.

The silicocarbonatites have elevated SiO_2, TiO_2, Al_2O_3, $(FeO)_t$, MgO, K_2O, P_2O_5, Ni, Co, Cr, V, Th and HFSE and have lower CaO than the calcio- and magnesiocarbonatites (Figs 3 and 4), which could be explained by silification of calciocarbonatites, similar to those from western Tamazert with elevated incompatible element abundances, by silica-rich hydrothermal fluids. This conclusion is supported by the elevated stable isotope ratios in the silicocarbonatites and the presence of secondary quartz and other silicate phases in these samples. The stable isotope ratios, however, are not as high as those observed in the magnesiocarbonatites, making the magnesiocarbonatites an unlikely parent for the silicocarbonatites, despite their nearly identical radiogenic isotopic compositions. There is, however, some question as to whether hydrothermal fluids could cause the observed HFSE enrichment. Therefore as an alternative to silification through hydrothermal fluids, the silicocarbonatites may originally have been mixtures of calciocarbonatite and silicic melts, as silicic melts are enriched in the same major and trace elements as the silicocarbonatites. The elevated stable isotopic compositions, however, suggest that some crustal interaction or recrystallization took place. The eastern calciocarbonatites that have not interacted with the Jurassic limestones (those with high-Sr and low-Sr isotope ratios) have similar Sr and Nd isotopic compositions to the magnesio- and silicocarbonatites. The Pb isotope ratios are also very similar, except that the magnesio- and silicocarbonatites have slightly higher $^{206}Pb/^{204}Pb$ isotope ratios. The slightly elevated $^{206}Pb/^{204}Pb$ isotope ratios of the silicocarbonatites compared with the eastern calciocarbonatites could be derived from silicate rocks in the complex, similar to the magnesiocarbonatites. Alternatively, these isotopic compositions may reflect those of the carbonatite sources. Excluding the high-$^{87}Sr/^{86}Sr$ isotope eastern Tamazert calciocarbonatite samples, the remaining carbonatites form positive arrays on Pb isotope diagrams and a negative correlation on the $^{206}Pb/^{204}Pb$ vs $^{143}Nd/^{144}Nd$ isotope diagram, with the eastern Tamazert calcio-, magnesio- and silicocarbonatites having more radiogenic Pb and Nd isotope ratios than the western Tamazert carbonatites. These geographical differences are still present if only calciocarbonatites with mantle O and C isotope ratios are considered, indicating a difference in the mantle source composition of the carbonatites from the different areas. The eastern Tamazert carbonatites are derived from a higher time-integrated U/Pb (HIMU)-type source and the western Tamazert carbonatites from a more enriched mantle I (EMI)-type source, similar to what has been proposed for the carbonatites in the Cape Verde Islands.

Origin of carbonatite melts

Carbonatite petrogenesis remains the subject of considerable debate. Various petrogenetic models have been proposed, ranging from direct partial melting of a carbonated peridotitic mantle source (Le Bas, 1981; Wyllie *et al.*, 1996), through fractional crystallization and/or liquid immiscibility of mantle-derived, CO_2-bearing, nephelinitic or melilitic parental melts (Gittins, 1989; Bell, 1998; Halama *et al.*, 2005), to intrusion-induced anatexis of limestone through volatile fluxing (Lentz, 1999) as recently reviewed by Woolley (2003) and Mitchell (2005). The key features that may potentially be used to distinguish primary carbonatitic melts from those derived from differentiation of parental silicate melts have been discussed by various workers (Bell, 1998; Harmer & Gittins, 1998; Lee & Wyllie, 1998; Bell & Rukhlov, 2004).

Petrological experiments suggest that primary carbonatitic melts may be produced by very low-degree partial melting of carbonated mafic or ultramafic lithologies (eclogite or peridotite) between 2·1 and 3·1 GPa and 930 and 1080°C (Wallace & Green, 1988; Bailey, 1993; Sweeney, 1994; Yaxley & Green, 1996). Carbonatitic melts produced by low-degree partial melting of carbonated eclogite show a larger variation in CaO content (from magnesio- to calciocarbonatites) than peridotite-derived melts (Dalton & Wood, 1993; Hammouda, 2003; Dasgupta *et al.*, 2005), with residual near-solidus carbonatitic melt becoming less calcic with increasing pressure (Dasgupta & Hirschmann, 2007). The resulting melts are usually dolomitic with CaO and MgO contents dependent on the source composition and P–T conditions of partial melting (e.g. the stability of dolomite solid solution in the residue) (Dalton & Wood, 1993; Dasgupta *et al.*, 2004, 2005; Gudfinnsson & Presnall, 2005; Dasgupta & Hirschmann, 2007; Brey *et al.*, 2008), and may evolve towards calciocarbonatitic compositions through wall-rock interaction

when migrating through peridotite (Dalton & Wood, 1993). This observation could explain why the least altered oceanic and continental carbonatites on the NW African plate are calciocarbonatites (Hoernle & Tilton, 1991; Hoernle *et al.* 2002; this study). Accordingly, carbonatites appear to be the end-products of the complex evolution of primary mantle-derived liquids that may involve reactions with mantle and/or crustal wall-rocks, crystal fractionation and the loss of volatile and alkali-rich components (Dalton & Wood, 1993; Harmer & Gittins, 1997; Bühn & Rankin, 1999; Harmer, 1999; Nielson & Veksler, 2002). Reconstructing these processes in the petrogenesis of the Tamazert carbonatites is beyond the scope of this study. Below we compare the Tamazert carbonatites with other African carbonatites and with carbonatites and silicate igneous rocks from the Canary and Cape Verde Islands to gain additional insights into the mantle sources and origin of these rocks.

Comparison of Tamazert with other African carbonatites and NW African silicate igneous rocks

Excluding the crustally contaminated low-Sr, high-$^{87}Sr/^{86}Sr$ calciocarbonatites from eastern Tamazert, the other Tamazert carbonatites form a near-vertical array on a $^{87}Sr/^{86}Sr$ vs $^{143}Nd/^{144}Nd$ isotope diagram with a slightly negative slope, a nearly horizontal array on a $^{206}Pb/^{204}Pb$ vs $^{87}Sr/^{86}Sr$ isotope diagram with slight negative slope, and positive arrays on $^{206}Pb/^{204}Pb$ vs $^{207}Pb/^{204}Pb$, $^{208}Pb/^{204}Pb$ and $^{143}Nd/^{144}Nd$ diagrams. These arrays remain even if only samples with mantle O and C isotopic compositions are considered. These arrays indicate the presence of both HIMU- and EMI-type components in the mantle source of the Tamazert carbonatites, similar to what has been observed in the Cape Verde Islands (Figs 5 and 7). The carbonatite data from Tamazert, the Cape Verdes and Fuerteventura, Canary Islands, taken together fall along similar arrays to the Tamazert carbonatite data, which holds true even if only calciocarbonatites with mantle O and C isotopic compositions are considered. The close similarity in carbonatite compositions between the Cape Verdes, Canaries and Tamazert suggest a common source(s) for these carbonatites. Although other African carbonatites (from eastern and southern Africa) also form arrays between HIMU- and EMI-type components, their arrays are shifted to higher $^{87}Sr/^{86}Sr$ and $^{207}Pb/^{204}Pb$ and lower $^{143}Nd/^{144}Nd$ at a given $^{206}Pb/^{204}Pb$ isotope ratio (Fig. 8). The EMI component involved in the petrogenesis of Eastern Canary Island and southern Cape Verde Island lavas was suggested to result from the involvement of recycled African subcontinental lithosphere (Hoernle & Tilton, 1991; Hoernle *et al.*, 2002). It is also likely that the weak EMI influence on the low-$^{87}Sr/^{86}Sr$, low-Δ7/4Pb crustally uncontaminated Tamazert calciocarbonatites results from interaction with the underlying NW African lithospheric mantle.

Low-$^{87}Sr/^{86}Sr$, low-Δ7/4Pb igneous rocks from continental NW Africa such as the *c.* 42 Ma Tamazert carbonatites, basanites from the Rekkame plateau (age corrected to 43 Ma) and Miocene and Quaternary Middle Atlas basanites form a group together with the oceanic igneous rocks from the Canary and Cape Verde Islands (Fig. 8). The Tamazert, Rekkame, Atlas and Cape Verde igneous rocks overlap with the Holocene Canary Island lavas in the Pb isotope diagram (Fig. 8b). All these samples have relatively low $^{87}Sr/^{86}Sr$ (Fig. 8a), plot on or below the NHRL, and stem from both continental and oceanic intraplate areas of the NW African plate. Therefore, the similarity in the Sr–Nd–Pb isotope ratios of these igneous rocks may point to a common sublithospheric source.

Is there a mantle plume beneath NW Africa?

The similarity of the geochemical and isotopic compositions of both carbonatites and ocean island basalts (OIBs) has led many researchers to argue that carbonatites are associated with mantle upwellings and in many cases with mantle plumes (Bell, 2001, and references therein). For the origin of the NW African alkaline igneous provinces, several variations of the plume model have been proposed and recently revisited, including: (1) a long-lived large mantle upwelling lasting since the Triassic (Oyarzún *et al.*, 1997; Anguita & Hernán, 2000); (2) a large-scale sheet-like mantle upwelling emanating from the eastern North Atlantic (Hoernle *et al.*, 1995); (3) a small Cenozoic asthenospheric plume similar to those observed in the West European Alpine Foreland (Zeyen *et al.*, 2005); (4) a shallow mantle upwelling during middle to late Miocene time, during a period of relative tectonic quiescence (Missenard *et al.*, 2006). The Tamazert carbonatites are highly enriched in incompatible trace elements and have isotope signatures similar to many OIBs worldwide. Based on the trace element and C–O–Sr–Nd isotopic composition of lamprophyres and two carbonatite samples from Tamazert, it was suggested that the various rock-types of the complex could have been derived from a mantle plume (Bernard-Griffiths *et al.*, 1991).

There is, however, geological and geophysical evidence arguing against the presence of a deep-rooted mantle plume beneath northwestern Africa. Magma supply rates are low compared with hotspot areas associated with mantle plumes rising from the core–mantle boundary as observed in seismic tomography models (e.g. Canary Islands, Cape Verdes and Azores) (Montelli *et al.*, 2006). The igneous activity in NW Africa is not continuous and did not produce a line of volcanoes showing gradual age progression, as observed, for example, for the Canary hotspot track (Fig. 1) (Geldmacher *et al.*, 2005). Field relationships show that the emplacement of the Tamazert complex

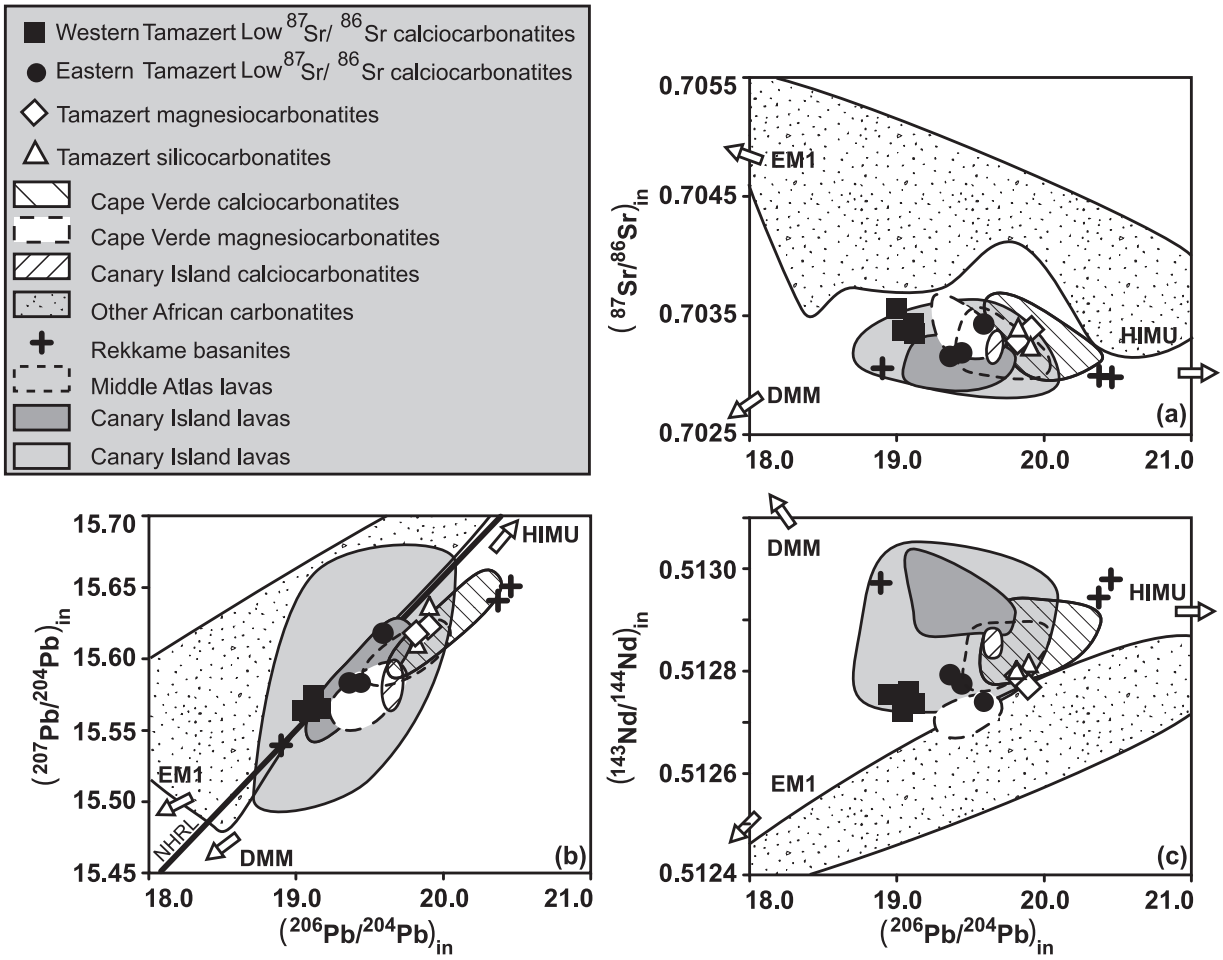

Fig. 8. Sr–Nd–Pb isotopic composition of high-Sr, low-$^{87}Sr/^{86}Sr$ Tamazert calciocarbonatites compared with continental African carbonatites (from East and South Africa) and other carbonatites and silicate lavas from the NW African plate such as oceanic carbonatites and mafic lavas from the Cape Verde and Canary Islands and Atlas silicate mafic lavas (Rekkame, Middle Atlas). Most of the calciocarbonatites have mantle O and C isotopic compositions. The magnesio- and silicocarbonaties from the Cape Verdes and Tamazert do not have mantle-like O and C isotopic compositions but may reflect the Sr–Nd–Pb isotopic composition of their mantle sources. Data sources: East and South African continental carbonatites from Nelson *et al.* (1988), Simonetti & Bell (1994), Paslick *et al.* (1995), Kalt *et al.* (1997), Harmer *et al.* (1998), Le Roex & Lanyon (1998) and Bell & Tilton (2001); Cape Verde and Canary Islands carbonatites from Hoernle & Tilton (1991) and Hoernle *et al.* (2002); Rekkame basanites from Duggen *et al.* (2005); low Δ7/4Pb Middle Atlas basanites from Duggen *et al.* (2009); mantle endmembers DMM, EMI and HIMU from Zindler & Hart (1986).

is structurally controlled (Mattauer *et al.*, 1977; Kchit, 1990) and that the emplacement of the carbonatitic magmas took place in response to tectonic regime transition from transpression to transtension at the Paleocene–Eocene boundary as a result of a shift in eastward motion of the African and European plates (see below). A similar model has been proposed for the genesis of Himalayan carbonatites (Hou *et al.*, 2006). Moreover, the Tamazert and other NW African igneous rocks are not part of the Canary hotspot track, which is located on the oceanic side of the African plate (Geldmacher *et al.*, 2005; see Fig. 1). Recent P- and S-wave seismic tomographic studies show that the well-resolved seismic anomalies beneath the Canary Islands do not extend beneath Africa at depths between 300 and 600 km (Montelli *et al.*, 2004, 2006), strongly arguing against a deep upwelling beneath NW Africa and the Tamazert complex. A geochemical similarity, however, exists between silicate and carbonatitic lavas from intraplate igneous areas both on the continental and oceanic part of the NW African plate since the Eocene. Regionally, Lustrino & Wilson (2007) concluded that there is no need to invoke the involvement of a single or multiple deep mantle plumes to explain the Cenozoic circum-Mediterranean anorogenic magmatism.

Model for the origin of the Tamazert carbonatites

Previous investigations have shown that the High Atlas system resulted from the tectonic inversion of Late Triassic to Early Liassic extensional basins, genetically related to

the opening of the Tethyan and Central Atlantic oceans (e.g. Piqué *et al.*, 2000). The inversion of the Mesozoic basins occurred from Cenozoic to present times in response to the convergence between Africa and Europe (Mattauer *et al.*, 1977; Giese & Jacobshagen, 1992). Over the past 45 Myr, collision of the African and European plates has deformed the former rift (Gomez *et al.*, 2000). Recent geophysical data show the existence of a 600 km long and 200 km wide channel of abnormally thin lithosphere (Fig. 1), extending from the passive continental margin near the Canary Islands and beneath the Atlas Mountains to the Mediterranean (see Fig. 1 for the location of this subcontinental trans-Atlas corridor) (Teixell *et al.*, 2005; Zeyen *et al.*, 2005; Fuella Urchulutegui *et al.*, 2006; Missenard *et al.*, 2006).

Several studies have proposed delamination of subcontinenal lithosphere under NW Africa to explain the volcanism, the intermediate depth of regional earthquakes and the rapid uplift of the Atlas Mountains (Seber *et al.*, 1996; Ramdani, 1998; Duggen *et al.*, 2005, 2009). Delamination may be triggered by lithospheric shortening. Evaluation of tectonic shortening ratios in both the High and Middle Atlas has yielded values ranging from 10 to 45% (Brede *et al.*, 1992; Zouine, 1993; Beauchamp *et al.*, 1999; Gomez *et al.*, 2000; Teixell *et al.*, 2003), with most of the values clustering around 20%. Ratios below 20% were considered insufficient to cause delamination and were used to argue against a delamination model for the formation of the Trans-Atlas NW African sublithospheric corridor. The Atlas system, however, corresponds to a failed Early Mesozoic rift structure prone to delamination upon compression, even at moderate amounts of shortening. Furthermore, shortening is not a necessary condition to initiate lithospheric thinning and subsequent delamination. Lateral density contrasts within the upper mantle as small as 1% are sufficient to generate extensional stresses large enough to drive gravitational Rayleigh–Taylor instabilities and consequently promote delamination or lithospheric removal (Elkins-Tanton, 2005).

Rifting-related Triassic dolerite–diabase and Jurassic gabbro bodies are widespread in the High Atlas (Hailwood & Mitchell, 1971; Chévrement, 1975; Zayane, 1992; Beraâouz *et al.*, 1994). Gravity data show the existence of such lithologies at minimum depths of 10 and 26 km (Ayarza *et al.*, 2005). Buried at such depths and deeper (>50 km), gabbro and dolerite–diabase rocks may metamorphose to higher-temperature and -pressure mineral assemblages, producing a higher-density eclogitic rock (e.g. 3·3–3·5 g/cm^3; Leech, 2001). The density contrast between the newly formed eclogite and the laterally adjacent materials will drive a gravitational instability, which consequently promotes delamination. Numerical models indicate that delamination can occur in less than 5 Myr (Elkins-Tanton & Hager, 2000). This timescale is in good agreement with the 4 Myr calculated as the duration of the magmatic episodes that occurred at Tamazert (42–38 Ma); coincident with the European–African collisional event. During Paleocene–Eocene times, the African and European plates drifted eastward (Brede *et al.*, 1992), causing a reorientation of the compressional stress, and consequently shifting the stress regime from transpressional to transtensional at the Eocene–Oligocene boundary (*c.* ~40 Ma), contemporaneously with the emplacement of the Tamazert complex. Accordingly, Kchit (1990) assumed syntectonic emplacement for the Tamazert intrusion along two sets of crustal fractures caused by the same SW–NE sinistral shearing. Convergence rates between the African and European plates have increased since the Miocene (Brede *et al.*, 1992), resulting in the production of large volumes of anorogenic alkaline effusive rocks with minor pyroclastic deposits and high-level intrusions that cover much of the Middle and High Atlas domains (Fig. 1).

Based on the geochemical similarity between silicate volcanic rocks erupted above the corridor in the Middle Atlas and in northern Morocco near the Mediterranean, Duggen *et al.* (2009) proposed that plume material upwelling beneath the Canary Islands flowed laterally beneath NW Africa through the 'Trans-Atlas corridor'. The plume material flowing through the corridor melts by decompression as the lithosphere thickness above the corridor becomes thinner, causing volcanism in the Middle Atlas and areas in northern Morocco near the Mediterranean. The similarity in trace element and Sr–Nd–Pb isotopic composition between the Tamazert, Canary and Cape Verde carbonatites, in particular when compared with carbonatites from eastern and southern Africa, is startling, further supporting a strong link between the Canary Islands and Cenozoic volcanism in northwesternmost Africa (northern Morocco). The Eocene Tamazert carbonatites represent the oldest magmatic rocks above the lithospheric corridor recognized thus far that have Sr–Nd–Pb isotopic compositions consistent with being derived from inflowing carbonated Canary mantle plume material. Therefore we propose that at least part of the lithospheric corridor may have been open by ~42 Ma ago, consistent with the African–European collisional event being the cause of the formation of the sublithospheric corridor. Finally, we briefly address the close similarity between both the silicate and carbonatitic rocks from the Canary Islands, northern Morocco and the Cape Verde Islands. Interestingly, in the most recent seismic tomographic images of the mantle beneath this region, the Canary and Cape Verde low-velocity anomalies are connected at depths of about 1000 km, suggesting that the plumes feeding both island groups and volcanism above the 'Trans-Atlas corridor' are ultimately derived from a common deep-mantle source (Montelli *et al.*, 2006),

consisting of recycled oceanic magmatic and carbonate crustal rocks (Hoernle *et al.*, 2002).

CONCLUSIONS

Carbonatites from the Eocene Tamazert complex in the Moroccan High Atlas Range include calcio-, magnesio- and silicocarbonatites. They are all enriched in LREE and LILE (Cs, Rb, Ba, U and Th), but show relative depletion in HFSE. In the C–O isotope diagram, the Tamazert carbonatites form an array between the mantle box and marine sediments.

Two groups of calciocarbonatites exist in the eastern Tamazert complex: (1) a group with high Sr and Ba, mantle-like O and C isotopic compositions, and relatively unradiogenic Sr but radiogenic Nd and Pb isotopic compositions; (2) a group with low Sr and Ba, elevated O and C isotopic compositions, and very radiogenic Sr and unradiogenic Nd, $^{206}Pb/^{204}Pb$ and $^{208}Pb/^{204}Pb$ isotopic compositions. The low-Sr calciocarbonatites are interpreted to have acquired their radiogenic isotopic compositions through interaction with Jurassic limestones and other crustal rocks, whereas the high-Sr calciocarbonatites are considered to reflect the composition of the primary carbonatite melts derived from the mantle.

The western Tamazert carbonatites, which have mantle-like C and O isotopic compositions, have distinct incompatible and isotopic compositions from the high-Sr, mantle-derived carbonatites from eastern Tamazert, indicating derivation from different mantle sources. Whereas the eastern Tamazert calciocarbonatites with high Sr have more HIMU-like radiogenic isotopic compositions, the western Tamazert carbonatites have more EM-like radiogenic isotopic compositions with slightly less radiogenic Nd and also less radiogenic Pb isotopic compositions.

The magnesio- and silicocarbonatites from eastern Tamazert have elevated O and C isotopic compositions indicating interaction with hydrothermal fluids rich in magnesium and silica. They have similar incompatible element characteristics to some calciocarbonatites and isotopic compositions similar to the eastern Tamazert carbonatites, except that they have slightly elevated $^{206}Pb/^{204}Pb$ isotope ratios. The slightly higher $^{206}Pb/^{204}Pb$ ratios could be derived from associated mafic and ultramafic silicate rocks with high U/Pb ratios, which are also likely to be the source of the magnesium and silica involved in forming the magnesio- and silicocarbonatites. These carbonatites are interpreted to have been derived from calciocarbonatite parent magmas that were altered within the crust by interaction with hydrothermal fluids.

The Tamazert calciocarbonatites with mantle-like O and C isotopic compositions have Sr–Nd–Pb isotope signatures distinct from eastern and southern African continental carbonatites but instead show remarkable geochemical similarities to (1) oceanic carbonatites from the Canary and Cape Verde Islands, and (2) other continental alkaline igneous rocks found in the Atlas system, such as the mafic silicate igneous rocks from the Eocene Rekkame and the Miocene and Quaternary Middle Atlas volcanic fields. The close similarity between the geochemistry of the Tamazert and Canary carbonatites and the lack of geophysical evidence for a mantle plume beneath the central High Atlas suggest derivation of the Tamazert carbonatites from the Canary plume, possibly as a result of flow of Canary plume-type mantle through a lithospheric corridor beneath northern Morocco. In this case, the sublithospheric corridor must have begun formed at least 45 Myr ago. The presence of geochemically very similar carbonatites in the central High Atlas, Canary Islands and Cape Verde Islands, combined with seismic tomographic data, argues for derivation from a common lower mantle (>1000 km depth) source.

ACKNOWLEDGEMENTS

We are grateful to Donald Sangster and Linda T. Elkins-Tanton for helpful comments on earlier versions of the manuscript. Thanks go to Dagmar Rau at IFM-GEOMAR for XRF analyses. The study was supported by the Moroccan Programme d'Appui à la Recherche Scientifique (PROTARS II/P23/33) and by a DAAD (German Academic Exchange Service) fellowship awarded to M.B. The project was further supported by the Deutsche Forschungsgemeinschaft (DU426/1-1 & 3-1 and HO1833/16-1 & 18-1) and a UK Royal Society/Leverhulme Trust Senior Research Fellowship to Matthew Thirlwall, allowing S.D. to stay for more than a year at RHUL.

REFERENCES

Agard, J. (1956*a*). Les ankaratrites et le volcanisme récent de la région de Zebzat (Haut Atlas de Midelt, Maroc). *Notes du Service Géologique du Maroc* **15**, 109–118.

Agard, J. (1956*b*). Les gîtes minéraux associés aux roches alcalines et aux carbonatites. *Sciences de la Terre* **4**(1–2), 103–151.

Agard, J. (1960). Les carbonatites et les roches à silicates et carbonates associés du massif de roches alcalines du Tamazeght (Haut Atlas de Midelt, Maroc) et les problèmes de leur genèse. *Proceedings of the 21st International Geological Congress, Norden, Norway* **13**, 293–303.

Agard, J. (1973). Carte géologique du complexe de roches alcalines à carbonatites de Tamazeght (Haut Atlas de Midelt, Maroc). *Notes et Mémoires du Service Géologique du Maroc* **248.**

Agard, J. (1977). Notice explicative de la carte géologique du complexe de roches alcalines à carbonatites du Tamazeght (Haut Atlas de Midelt, Maroc). *Compte Rendu d'Activité Annuelle.* Rabat: Direction de Géologie Rabat.

Aghchmi, E. M. (1984). Les carbonatites filoniennes de l'oued Tamazeght et leurs relations avec les métasyénites (Haut Atlas de Midelt, Maroc). PhD thesis, Université Paul Sabatier, Toulouse, 106 p.

Al-Haderi, M., Tayebi, M., Bouabdli, A. & El-Hanbali, M. (1998). Chronologie et conditions de mise en place des différents faciès

pétrographiques du complexe alcalin de Tamazert (Haut Atlas de Midelt, Maroc). *Africa Geoscience Review* **5**, 159–171.

Anderson, T. (1987). Mantle and crustal components in a carbonatitic complex, and the evolution of carbonatitic magmas: REE and isotopic evidence from the Fen complex, southeast Norway. *Chemical Geology* **65**, 147–166.

Anguita, F. & Hernán, F. (2000). The Canary Islands origin: a unifying model. *Journal of Volcanology and Geothermal Research* **103**, 1–26.

Anovitz, L. M. & Essene, E. J. (1987). Phse equilibria in the system $CaCO_3$–$MgCO_3$–$FeCO_3$. *Journal of Petrology* **28**, 389–414.

Ayarza, P., Alvarez-Lobato, F., Teixel, A., Arboleya, M. L., Tesón, E., Julivert, M. & Cherroud, M. (2005). Crustal structure under the central High Atlas Mountains (Morocco) from geological and gravity data. *Tectonophysics* **400**, 67–84.

Barker, D. S. (1989). Field relations of carbonatites. In: Bell, K. (ed.) *Carbonatites: Genesis and Evolution*. London: Unwin Hyman, pp. 38–69.

Bailey, D. K. (1992). Episodical alkaline igneous activity across Africa: implications for the causes of continental break-up. In: Storey, B. C., Alabaster, T. & Pankhurst, R. J. (eds) *Magmatism and the Causes of Continental Break-up. Geological Society, London, Special Publications* **68**, 91–98.

Bailey, D. K. (1993). Carbonate magma. *Journal of the Geological Society, London* **150**, 637–651.

Beauchamp, W., Allmendinger, R. W., Barazangi, M., Demnati, A., El Alji, M. & Dahmani, M. (1999). Inversion tectonics and evolution of the High Atlas Mountains of Morocco. *AAPG Bulletin* **80**, 1459–1482.

Bell, K., Blenkinsop, J., Cole, T. J. S. & Menagh, D. P. (1982). Evidence from Sr isotopes for long-lived heterogeneities in the upper mantle. *Nature* **298**, 251–253.

Bell, K. (1998). Radiogenic isotopes constraints on relationship between carbonatites and associated silicate rocks—a brief review. *Journal of Petrology* **39**(11–12), 1987–1996.

Bell, K., Kjarsgaard, B. A. & Simonetti, A. (1998). Carbonatites – into the twenty-first century. *Journal of Petrology* **39**, 1839–1845.

Bell, K. (2001). Carbonatites: relationships to mantle-plume activity. In: Ernest, R. E. & Buchan, K. L. (eds) *Mantle Plumes: Their Identification Through Time. Geological Society of America, Special Papers* **352**, 267–290.

Bell, K. & Tilton, G. R. (2001). Nd, Pb and Sr isotope compositions of East African carbonatites: evidence for mantle mixing and plume inhomogeneity. *Journal of Petrology* **37**, 1927–1945.

Bell, K. & Rukhlov, A. S. (2004). Carbonatite from the Kola Alkaline Province: origin, evolution and source characteristics. In: Wall, F. & Zaitsev, A. N. (eds) *Phoscorites and Carbonatites from Mantle to Mine: the Key Example of the Kola Alkaline Province. Mineralogical Society Series* **10**, 443–468.

Bellon, H. & Brousse, R. (1977). Le magmatisme périméditerranéen occidental. Essai de synthèse. *Bulletin de la Société Géologique de France* **7**, 469–480.

Beraâouz, E. H., Platevoet, B. & Bonin, B. (1994). Le magmatisme mésozoïque du Haut Atlas (Maroc) et l'ouverture de l'Atlantique central. *Comptes Rendus de l'Académie des Sciences, Série II* **318**, 1079–1085.

Bernard-Griffiths, J., Peucat, J.-J. & Ménot, R.-P. (1991). Isotopic (Rb–Sr, U–Pb and Sm–Nd) and trace element geochemistry of eclogites from the pan-African Belt: A case study of REE fractionation during high-grade metamorphism. *Lithos* **27**, 43–57.

Berrahma, M. & Hernandez, J. (1985). Nouvelles données sur le volcanisme trachytique hyperalcalin du volcan du Siroua (Anti-Atlas, Maroc). *Comptes Rendus de l'Académie des Sciences* **300**, 863–868.

Berrahma, M., Delaloye, M., Faure-Muret, A. & Rachdi, H. E. (1993). Premières données géochronologiques sur le volcanisme alcalin du Jbel Saghro, Anti-Atlas, Maroc. *Journal of African Earth Sciences* **17**(3), 333–341.

Bouabdli, A. (1987). Etude pétrologique et géochimique des lamprophyres et roches associées de la région de Tamazert (Haut Atlas de Midelt, Maroc). PhD thesis, Université de Montpellier, 195 p.

Bouabdli, A., Dupuy, C. & Dostal, J. (1988). Geochemistry of Mesozoic alkaline lamprophyres and related rocks from the Tamazert massif, High Atlas (Morocco). *Lithos* **22**, 43–58.

Bouabdli, A. & Liotard, J. M. (1992). Affinité kimbérlitique des lamprophyres ultramafiques du massif carbonatitique de Tamazert (Haut Atlas marocain. *Comptes Rendus de l'Académie des Sciences, Série II* **314**, 351–357.

Brede, R., Hauptmann, M. & Herbig, H.-G. (1992). Plate tectonics and the intracratonic mountain ranges in Morocco—The Mesozoic–Cenozoic development of the Central High Atlas and the Middle Atlas. *Geologische Rundschau* **81**, 127–141.

Brey, G. P., Bulatov, V. K., Girnis, A. V. & Lahaye, Y. (2008). Experimental melting of carbonated peridotite at 6–10 GPa. *Journal of Petrology* **49**, 797–821.

Bühn, B. (2008). The role of the volatile phase for REE and Y fractionation in low silica–carbonate magmas: implications from natural carbonatites, Namibia. *Mineralogy and Petrology* **92**, 453–470.

Bühn, B. & Rankin, A. H. (1999). Composition of natural, volatile-rich Na–Ca–REE–Sr carbonatitic fluid trapped in fluid inclusions. *Geochimica and Cosmochimica Acta* **63**, 3781–3797.

Chakhmouradian, A. R. (2006). High-field-strength elements in carbonatitic rocks: Geochemistry, crystal chemistry and significance for constraining the sources of carbonatites. *Chemical Geology* **235**, 138–160.

Charlot, R., Choubert, G., Faure-Muret, A. & Hamel, C. (1964). Age des aïounites du Maroc Nord-Oriental. *Comptes Rendus Sommaire de la Société Géologique de France* **9**, 401–402.

Chévrement, P. (1975). Les roches éruptives basiques des boutonnières de Tassent et Tasraft et leurs indices métallifères dans leur cadre géologique (Haut Atlas central, Maroc). PhD thesis, Université Claude Bernard, Lyon, 209 p.

Coulson, I. M., Goodenough, K. M., Pearce, N. J. G. & Leng, M. J. (2003). Carbonatites and lamprophyres of the Gardar Province—a 'window' to the sub-Gardar mantle? *Mineralogical Magazine* **67**, 855–872.

Craig, H. (1957). Isotopic standards for carbon and oxygen, correction factors for mass spectrometric analysis of carbon dioxide. *Geochimica et Cosmochimica Acta* **12**, 133–149.

Dalton, J. A. & Wood, B. J. (1993). The compositions of primary carbonate melts and their evolution through wallrock reaction in the mantle. *Earth and Planetary Science Letters* **119**, 511–525.

Dasgupta, R., Hirschmann, M. M. & Withers, A. C. (2004). Deep global cycling of carbon constrained by the solidus of anhydrous, carbonated eclogite under upper mantle conditions. *Earth and Planetary Science Letters* **227**, 73–85.

Dasgupta, R., Hirschmann, M. M. & Dellas, N. (2005). The effect of bulk composition on the solidus of carbonated eclogite from partial melting experiments at 3 GPa. *Contributions to Mineralogy and Petrology* **149**, 288–305.

Dasgupta, R. & Hirschmann, M. M. (2007). A modified iterative sandwich method for determination of near-solidus partial melt compositions. II. Application to determination of near-solidus melt compositions of carbonated peridotite. *Contributions to Mineralogy and Petrology* **154**, 647–661.

Deines, P. (1989). Stable isotope variations in carbonatites. In: Bell, K. (ed.) *Carbonatites, Genesis and Evolution*. London: Unwin Hyman, pp. 301–359.

Deines, P. & Gold, D. (1973). The isotopic composition of carbonatite and kimberlite carbonates and their bearing on the isotopic composition of deep-seated carbon. *Geochimica et Cosmochimica Acta* **37**, 1709–1733.

Dubar, G. (1939). Carte géologique provisoire du Haut Atlas de Midelt et notice explicative. *Notes et Mémoires du Service Géologique du Maroc* **59–59bis**.

Duggen, S., Hoernle, K., Hauff, F., Klügel, A., Bouabdellah, M. & Thirlwall, M. F. (2009). Flow of Canary mantle plume material through a subcontinental lithospheric corridor beneath Africa to the Mediterranean. *Geology* **37**, 283–286.

Duggen, S., Hoernle, K., van den Bogaard, P. & Garbe-Schönberg, D. (2005). Post-collisional transition from subduction- to intraplate-type magmatism in the westernmost Mediterranean: Evidence for continental-edge delamination of subcontinental lithosphere. *Journal of Petrology* **46**, 1155–1201.

Elkins-Tanton, L. T. (2005). Continental magmatism caused by lithospheric delamination. In: Foulger, G. R., Natland, J. H., Presnall, D. C. & Anderson, D. L. (eds) *Plates, Plumes, and Paradigms. Geological Society of America, Special Papers* **388**, 449–461.

Elkins-Tanton, L. T. & Hager, B. H. (2000). Melt intrusion as a trigger for lithospheric foundering and the eruption of the Siberian flood basalt. *Geophysical Research Letters* **27**, 3937–3940.

Frizon de Lamotte, D., Leturmy, P., Missenard, Y., Khomsi, S., Ruiz, G., Saddiqi, O., Guillocheau, F. & Michard, A. (2009). Mesozoic and Cenozoic vertical movements in the Atlas system (Algeria, Morocco, Tunisia): an overview. *Tectonophysics* **745**, 9–28.

Fullea Urchulutegui, J., Fernàndez, M. & Zeyen, H. (2006). Lithospheric structure in the Atlantic–Mediterranean transition zone (southern Spain, northern Morocco): a simple approach from regional elevation and geoid data. In: Frizon de Lamotte, D., Saddiqi, O. & Michard, A. (eds) *Some Recent Developments in the Maghreb Geodynamics. Comptes Rendus Géosciences* **335**, 140–151.

Geldmacher, J., Hoernle, K., van den Bogaard, P., Duggen, S. & Werner, R. (2005). New $^{40}Ar/^{39}Ar$ age and geochemical data from seamounts in the Canary and Madeira Volcanic Provinces: A contribution to the 'Great Plume Debate'. *Earth and Planetary Science Letters* **237**, 85–101.

Giese, P. & Jacobshagen, V. (1992). Tectonic inversion of intracontinental ranges: High and Middle Atlas, Morocco. *Geologische Rundschau* **81**, 249–259.

Gittins, J. (1989). The origin and evolution of carbonatite magmas. In: Bell, K. (ed.) *Carbonatites: Genesis and Evolution*. London: Unwin Hyman, pp. 580–600.

Gittins, J. & Harmer, R. E. (1997). What is ferrocarbonatite? A revised classification. *Journal of African Earth Sciences* **25**, 159–168.

Gomez, F., Beauchamp, W. & Barazangi, M. (2000). Role of the Atlas Mountains (northwest Africa) within the African–Eurasian plate-boundary zone. *Geology* **28**, 775–778.

Gudfinnsson, G. H. & Presnall, D. C. (2005). Continous gradations among primary carbonatitic, kimberlitic, melititic, basaltic, picritic, and komatiitic melts in equilibrium with garnet lherzolite at 3–8 GPa. *Journal of Petrology* **8**, 1645–1659.

Hailwood, E. A. & Mitchell, J. G. (1971). Palemagnetic and radiometric dating results from Jurassic intrusion in south Morocco. *Geophysical Journal of the Royal Astronomical Society* **24**, 351–364.

Halama, R., Vennemann, T., Siebel, W. & Markl, G. (2005). The Gronnedal–Ika carbonatite–syenite complex, South Greenland: carbonatite formation by liquid immiscibility. *Journal of Petrology* **46**, 191–217.

Hammouda, T. (2003). High-pressure melting of carbonated eclogite and experimental constraints on carbon recycling and storage in the mantle. *Earth and Planetary Science Letters* **214**, 357–368.

Harmand, C. & Cantagrel, J. M. (1984). Le volcanisme alcalin tertiaire et quaternaire du Moyen Atlas (Maroc): chronologie K/Ar et cadre géodynamique. *Journal of African Earth Sciences* **2**, 51–55.

Harmer, R. E. & Gittins, J. (1997). The origin of dolomitic carbonatites: field and experimental constraints. *Journal of African Earth Sciences* **25**, 5–28.

Harmer, R. E. & Gittins, J. (1998). The case for primary mantle-derived carbonatite magma. *Journal of Petrology* **39**, 1895–1903.

Harmer, R. E., Lee, C. A. & Eglington, B. M. (1998). A deep mantle source for carbonatite magmatism: evidence from the nephelinites and carbonatites of the Buhera district, SE Zimbabwe. *Earth and Planetary Science Letters* **158**, 131–142.

Harmer, R. E. (1999). The petrogenetic association of carbonatite and alkaline magmatism: constraints from the Spitskop Complex, South Africa. *Journal of Petrology* **40**, 525–548.

Hart, S. R. (1984). A large-scale isotope anomaly in the Southern Hemisphere mantle. *Nature* **309**, 753–757.

Hernandez, J. & Bellon, H. (1985). Chronologie K-Ar du volcanisme miocène du Rif oriental (Maroc): implications tectoniques et magmatologiques. *Revue Géologie Dynamique et Géographie Physique Paris* **262**, 85–94.

Hoernle, K. & Tilton, G. (1991). Sr–Nd–Pb isotope data for Fuerteventura (Canary Islands) basal complex and subaerial volcanics: applications to magma genesis and evolution. *Schweizerische Mineralogische und Petrographische Mitteilungen* **71**, 5–21.

Hoernle, K., Zhang, Y. S. & Graham, D. (1995). Seismic and geochemical evidence for large-scale mantle upwelling beneath the eastern Atlantic and western central Europe. *Nature* **374**, 34–39.

Hoernle, K., Tilton, G., Le Bas, M. J., Duggen, S. & Garbe-Schönberg, D. (2002). Geochemistry of oceanic carbonatites compared with continental carbonatites: mantle recycling of oceanic crustal carbonate. *Contributions to Mineralogy and Petrology* **142**, 520–542.

Hitzman, M. W., Oreskes, N. & Einaudi, M. T. (1992). Geological characteristics and tectonic setting of Proterozoic iron oxide (Cu–U–Au–REE) deposits. *Precambrian Research* **58**, 241–287.

Hogarth, D. D. (1989). Pyrochlore, apatite and amphibole: distinctive minerals in carbonatite. In: Bell, K. (ed.) *Carbonatites: Genesis and Evolution*. London: Unwin Hyman, pp. 105–148.

Hornig-Kjarsgaard, I. (1998). Rare earth elements in sövitic carbonatites and their mineral phases. *Journal of Petrology* **39**, 2105–2122.

Hou, Z., Tian, S., Yuan, Z., Xie, Y., Yin, S., Yi, L., Fei, H. & Yang, Z. (2006). The Himalayan collision zone carbonatites in western Sichuan, SW China: petrogenesis, mantle source and tectonic implication. *Earth and Planetary Science Letters* **244**, 234–250.

Kadar, M. (1984). Minéralogie et implications pétrologiques des pegmatites des syénites néphéliniques du massif alcalin du Tamazeght (Haut Atlas de Midelt, Maroc). PhD thesis, Université de Toulouse, 146 p.

Kalt, A., Hegner, E. & Satir, M. (1997). Nd, Sr, and Pb isotopic evidence for diverse lithospheric mantle sources of East African Rift carbonatites. *Tectonophysics* **278**, 31–45.

Kchit, A. (1990). Le complexe plutonique alcalin du Tamazert, Haut Atlas de Midelt (Maroc). Pétrologie et structurologie. PhD thesis, Université de Toulouse, 302 p.

Keller, J. & Hoefs, J. (1995). Stable isotope characteristics of recent natrocarbonatites from Oldoinyo Lengai. In: Bell, K. & Keller, J.

(eds) *Carbonatite Volcanism: Oldoinyo Lengai and the Petrogenesis of Natrocarbonatites*. Berlin: Springer, pp. 113–123.

Keppler, H. (2003). Water solubility in carbonatite melts. *American Mineralogist* **88**, 1822–1824.

Khadem-Allah, B. (1993). Syénites et pegmatites néphéliniques du complexe alcalin du Tamazert (Haut Atlas de Midelt, Maroc). PhD thesis, Université de Toulouse, 240 p.

Khadem-Allah, B., Monchoux, P., Fontan, F., Béziat, D. & Kadar, M. (1996). Clinopyroxènes des syénites nephéliniques du Tamazeght (Haut Atlas de Midelt). *Comptes Rendus de l'Académie des Sciences, Série IIa* **323**, 841–847.

Khadem-Allah, B., Fontan, F., Kadar, M., Monchoux, P. & Sørensen, H. (1998). Reactions between agpaitic nepheline syenitic melts and sedimentary carbonate rocks, exemplified by the Tamazeght complex, Morocco. *Geochemistry International* **36**, 569–581.

Klein, J. L. & Harmand, C. (1985). Le volcanisme de la région Zebzate: âge et relations avec le complexe alcalin à carbonatites du Tamazert (Haut Atlas de Midelt, Maroc). In: *110ème Congrès National des Sociétés Savantes. Montpellier Sci. Fascicule* **VI**, 147–152.

Le Bas, M. J. (1981). Carbonatite magmas. *Mineralogical Magazine* **44**, 133–140.

Le Bas, M. J. & Srivastava, R. K. (1989). The mineralogy and geochemistry of the Mandwara carbonatite dykes, Sirohi district Rajasthan, India. *Neues Jahrbuch für Mineralogie, Abhandlungen* **160**, 207–227.

Lee, W.-J. & Wyllie, P. J. (1998). Petrogenesis of carbonatite magmas from mantle to crust, constrained by the system CaO–$(MgO + FeO^*)$–$(Na_2O + K_2O)$–$(SiO_2 + Al_2O_3 + TiO_2)$–$CO_2$. *Journal of Petrology* **39**, 495–517.

Leech, M. L. (2001). Arrested orogenic development: eclogitization, delamination and tectonic collapse. *Earth and Planetary Science Letters* **185**, 149–159.

Le Maitre, R. W. (ed.) (2002). *Igneous Rocks. A Classification and Glossary of Terms. Recommendations of the International Union of Geological Sciences Subcommission on the Systematics of Igneous Rocks*. Cambridge: Cambridge University Press, 236 p.

Lentz, D. R. (1999). Carbonatite genesis: a reexamination of the role of intrusion-related pneumatolytic skarn process in limestone melting. *Geology* **27**, 335–338.

Le Roex, A. P. & Lanyon, R. (1998). Isotope and trace element geochemistry of Cretaceous Damaraland lamprophyres and carbonatites, northwestern Namibia: evidence for plume–lithosphere interactions. *Journal of Petrology* **39**, 1117–1146.

Lustrino, M. & Wilson, M. (2007). The circum-Mediterranean anorogenic Cenozoic Igneous Province. *Earth-Science Reviews* **81**, 1–65.

Marks, M. A. W., Shilling, J., Coulson, I. M., Wenzel, T. & Markl, G. (2008). The alkaline–peralkaline Tamazeght complex, High Atlas mountains, Morocco: mineral chemistry and petrological constraints for derivation from a compositionally heterogeneous mantle source. *Journal of Petrology* **49**, 1097–1131.

Mattauer, M., Tappopnier, P. & Proust, F. (1977). Sur les mécanismes de formation des chaînes intracontinentales. L'exemple des chaînes atlasiques du Maroc. *Bulletin de la Société Géologique de France* **7**, 521–526.

Missenard, Y., Zeyen, H., Frizon de Lamotte, D., Leturmy, P., Petit, C., Sébrier, M. & Saddiqi, O. (2006). Crustal versus asthenospheric origin of relief of the Atlas Mountains of Morocco. *Journal of Geophysical Research* **111**, 1–13.

Mitchell, R. H. (2005). Carbonatites, carbonatites and carbonatites. *Canadian Mineralogist* **43**, 2049–2068.

Montelli, R., Nolet, G., Dahlen, F. A., Masters, G., Engdahl, E. R. & Hung, S.-H. (2004). Finite-frequency tomography reveals a variety of plumes in the mantle. *Science* **303**, 338–343.

Montelli, R., Nolet, G., Dahlen, F. A. & Masters, G. (2006). A catalogue of deep mantle plumes: new results from finite-frequency tomography. *Geochemistry, Geophysics, Geosystems* **7**, Q11007.

Mourtada, S. (1997). Pétrogenèse des carbonatites et contribution à l'étude des minéralisations associées: exemple du complexe alcalin de Tamazert (Haut Atlas marocain). PhD thesis, Université de Clermont-Ferrand, 320 p.

Mourtada, S., Le Bas, M. J. & Pin, C. (1997). Pétrogenèse des magnésio-carbonatites du complexe de Tamazert (Haut Atlas marocain). *Comptes Rendus de l'Académie des Sciences* **325**, 559–564.

Nelson, D. R., Chivas, A. R., Chappell, B. W. & McCullogh, M. T. (1988). Geochemical and isotopic systematics in carbonatites and implications for the evolution of ocean-island sources. *Geochimica et Cosmochimica Acta* **52**, 1–17.

Nielson, T. F. D. & Veksler, I. V. (2002). Is natrocarbonatite a cognate fluid condensite? *Contributions to Mineralogy and Petrology* **142**, 425–435.

Oyarzún, R., Doblas, M., López-Ruiz, J. & Cebriá, J. M. (1997). Opening of the central Atlantic and asymmetric mantle upwelling phenomena: Implications for long-lived magmatism in western North Africa and Europe. *Geology* **25**, 727–730.

Paslick, C., Halliday, A., James, D. & Dawson, J. B. (1995). Enrichment of the continental lithosphere by OIB melts: Isotopic evidence from the volcanic province of northern Tanzania. *Earth and Planetary Science Letters* **130**, 109–126.

Piqué, A., Charroud, M., Laville, E., Aït Brahim, L. & Amrhar, M. (2000). The Tethys southern margin in Morocco and Cenozoic evolution of the Atlas domain. In: *Peri-Tethys Memoir 5: New Data on Peri-Tethys Sedimentary Basins. Mémoires du Muséum National de l'Histoire Naturelle de Paris* **182**, 93–106.

Platt, R. G. & Woolley, A. R. (1990). The carbonatites and fenites of Chipman lake, Ontario. *Canadian Mineralogist* **28**, 241–250.

Rachdi, H., Berrahma, M., Delalolye, M., Faure-Muret, A. & Dahmani, M. (1997). Le volcanisme tertiaire du Rekkame (Maroc): pétrologie, géochimie et géochronologie. *Journal of African Earth Sciences* **24(3)**, 259–269.

Ramdani, F. (1998). Geodynamic implications of intermediate-depth earthquakes and volcanism in the intraplate Atlas mountains (Morocco). *Physics of the Earth and Planetary Interiors* **108**, 245–260.

Salvi, S., Fontan, F., Monchoux, P., Williams-Jones, A. E. & Moine, B. (2000). Hydrothermal mobilization of high field strength elements in alkaline igneous systems: evidence from the Tamazeght Complex (Morocco). *Economic Geology* **95**, 559–576.

Schilling, J., Marks, M. A. W., Wenzel, T. & Markl, G. (2009). Reconstruction of magmatic to subsolidus processes in an agpaitic system using eudialyte textures and composition: a case study from Tamazeght, Morocco. *Canadian Mineralogist* **47**, 351–365.

Seber, D., Barazangi, M., Tadili, B. A., Ramdani, M., Ibenbrahim, A. & Sari, D. B. (1996). Three-dimensional upper mantle structure beneath the intraplate Atlas and interplate Rif mountains of Morocco. *Journal of Geophysical Research* **101**, 3125–3138.

Simonetti, A. & Bell, K. (1994). Nd, Pb and Sr isotopic data from the Napak carbonatite–nephelinite centre, eastern Uganda: an example of open-system crystal fractionation. *Contributions to Mineralogy and Petrology* **115**, 356–366.

Smith, M. P. & Henderson, P. (2000). Preliminary fluid inclusion constraints on fluid evolution in the Bayan Obo Fe–REE–Nb deposit, Inner Mongolia, China. *Economic Geology* **95**, 1371–1388.

Stoppa, F. & Lupini, L. (1993). Mineralogy and petrology of the Polino monticellite calciocarbonatite (Central Italy). *Mineralogy and Petrology* **49**, 213–231.

Sun, S.-s. & McDonough, W. F. (1989). Chemical and isotopic systematics of oceanic basalts: implications for mantle composition and processes. In: Saunders, A. D. & Norry, M. J. (eds) *Magmatism in the Ocean Basins*. Geological Society, London, Special Publications **42**, 313–345.

Sweeney, R. J. (1994). Carbonatite melt composition in the Earth's mantle. *Earth and Planetary Science Letters* **128**, 259–270.

Taylor, H. P., Frechen, J. & Degens, E. T. (1967). Oxygen and carbon isotopic studies of carbonatites from the Laacher See District, West Germany and the Alno District, Sweden. *Geochimica et Cosmochimica Acta* **31**, 407–430.

Teixell, A., Arboleya, M.-L., Charroud, M. & Julivert, M. (2003). Tectonic shortening and topography in the central High Atlas (Morocco). *Tectonics* **22**, 1051.

Teixell, A., Ayarza, P., Zeyen, H., Fernàndez, M. & Arboleya, M.-L. (2005). Effects of mantle upwelling in a compressional setting: the Atlas Mountains of Morocco. *Terra Nova* **17**, 456–461.

Tisserant, D., Thuizat, R. & Agard, J. (1976). Données géochronologiques sur le complexe de roches alcalines du Tamazeght (Haut Atlas de Midelt, Maroc). *Bulletin du Bureau de Recherches Géologiques et Minières* **3**, 279–283.

Todt, W., Cliff, R. A., Hanser, A. & Hofmann, A. W. (1996). Evaluation of a ^{202}Pb–^{205}Pb double spike for high precision lead isotope analyses. In: Basu, A. & Hart, S. (eds) *Earth Processes: Reading the Isotopic Code. Geophysical Monograph, American Geophysical Union* **95**, 437 p.

Wagner, C., Mokhtari, A., Deloule, E. & Chabaux, F. (2003). Carbonatite and alkaline magmatism in Taourirt (Morocco): petrological, geochemical and Sr–Nd-isotope characteristics. *Journal of Petrology* **44**, 937–965.

Wallace, M. E. & Green, D. H. (1988). An experimental determination of primary carbonatite magma composition. *Nature* **199**, 801–802.

Woolley, A. R. (1982). A disussion of carbonatite evolution and nomenclature, and the generation of sodic and potassic fenites. *Mineralogical Magazine* **46**, 13–17.

Woolley, A. R. (2003). Carbonatites: abundance, distribution and ages. 4th Eurocarb Workshop. In: Rosatelli, G. & Wall, F. (eds). *European Science Foundation, Abstract volume*, Lanzarote and Fuerteventura Canary Islands, Spain, pp. 72–73.

Wyllie, P. J., Jones, A. P. & Deng, J. (1996). Rare earth elements in carbonatite-rich melts from mantle to crust. In: Jones, A. P., Wall, F. & William, C. T. (eds) *Rare Earth Minerals: Chemistry, Origin and Ore Deposits*. London: Chapman & Hall, pp. 77–104.

Yaxley, G. M. & Green, D. H. (1996). Experimental reconstruction of sodic dolomitic carbonatite melts from metasomatised lithosphere. *Contributions to Mineralogy and Petrology* **124**, 359–369.

Zartman, R. E. & Doe, B. R. (1981). Plumbotectonics—the model. *Tectonophysics* **75**, 135–162.

Zayane, R. (1992). La série plutonique du Haut Atlas central marocain (région d'Imilchil): pétrographie et géochimie; aspects métamorphiques et structuraux de sa mise en place. Ph.D. thesis, Université de Bretagne occidentale, Brest, 201 p.

Zeyen, H., Ayarza, P., Fernàndez, M. & Rimi, A. (2005). Lithospheric structure under the western African–European plate boundary: A transect across the Atlas Mountains and the Gulf of Cadiz. *Tectonics* **24**, TC2001.

Zindler, A. & Hart, S. (1986). Chemical geodynamics. *Annual Review of Earth and Planetary Sciences* **14**, 493–571.

Zouine, E. M. (1993). Géodynamique récente du Haut Atlas. Evolution de sa bordure septentrionale et du Moyen-Atlas sud-occidental au cours du Cénozoïque. PhD thesis, Université de Rabat, 300 p.